

# Synthesis and Preclinical Evaluation of PSMA-Targeted $^{111}\text{In}$ -Radioconjugates Containing a Mitochondria-Tropic Triphenylphosphonium Carrier

Joana F. Santos, Maria T. Braz, Paula Raposinho, Frederik Cleeren, Irwin Cassells, Simon Leekens, Christopher Cawthorne, Filipa Mendes, Célia Fernandes, and António Paulo\*



Cite This: *Mol. Pharmaceutics* 2024, 21, 216–233



Read Online

ACCESS |

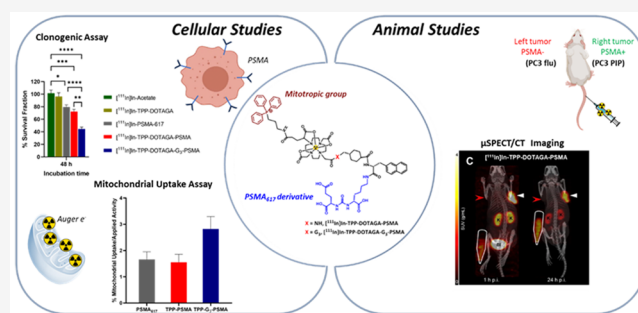
Metrics & More

Article Recommendations

Supporting Information

**ABSTRACT:** Nuclear DNA is the canonical target for biological damage induced by Auger electrons (AE) in the context of targeted radionuclide therapy (TRT) of cancer, but other subcellular components might also be relevant for this purpose, such as the energized mitochondria of tumor cells. Having this in mind, we have synthesized novel DOTA-based chelators carrying a prostate-specific membrane antigen (PSMA) inhibitor and a triphenyl phosphonium (TPP) group that were used to obtain dual-targeted  $^{111}\text{In}$ -radioconjugates ( $^{111}\text{In}$ -TPP-DOTAGA-PSMA and  $^{111}\text{In}$ -TPP-DOTAGA-G<sub>3</sub>-PSMA), aiming to promote a selective uptake of an AE-emitter radiometal ( $^{111}\text{In}$ ) by PSMA+ prostate cancer (PCa) cells and an enhanced accumulation in the mitochondria. These dual-targeted  $^{111}\text{In}$ -radiocomplexes are highly stable under physiological conditions and in cell culture media. The complexes showed relatively similar binding affinities toward the PSMA compared to the reference tracer  $^{111}\text{In}$ -PSMA-617, in line with their high cellular uptake and internalization in PSMA+ PCa cells. The complexes compromised cell survival in a dose-dependent manner and in the case of  $^{111}\text{In}$ -TPP-DOTAGA-G<sub>3</sub>-PSMA to a higher extent than observed for the single-targeted congener  $^{111}\text{In}$ -PSMA-617.  $\mu\text{SPECT}$  imaging studies in PSMA+ PCa xenografts showed that the TPP pharmacophore did not interfere with the excellent *in vivo* tumor uptake of the “golden standard”  $^{111}\text{In}$ -PSMA-617, although it led to a higher kidney retention. Such kidney retention does not necessarily compromise their usefulness as radiotherapeutics due to the short tissue range of the Auger/conversion electrons emitted by  $^{111}\text{In}$ . Overall, our results provide valuable insights into the potential use of mitochondrial targeting by PSMA-based radiocomplexes for efficient use of AE-emitting radionuclides in TRT, giving impetus to extend the studies to other AE-emitting trivalent radiometals (e.g.,  $^{161}\text{Tb}$  or  $^{165}\text{Er}$ ) and to further optimize the designed dual-targeting constructs.

**KEYWORDS:** dual-targeting, PSMA, mitochondria, radiopharmaceuticals, Auger electron emitters, cancer theranostics



## 1. INTRODUCTION

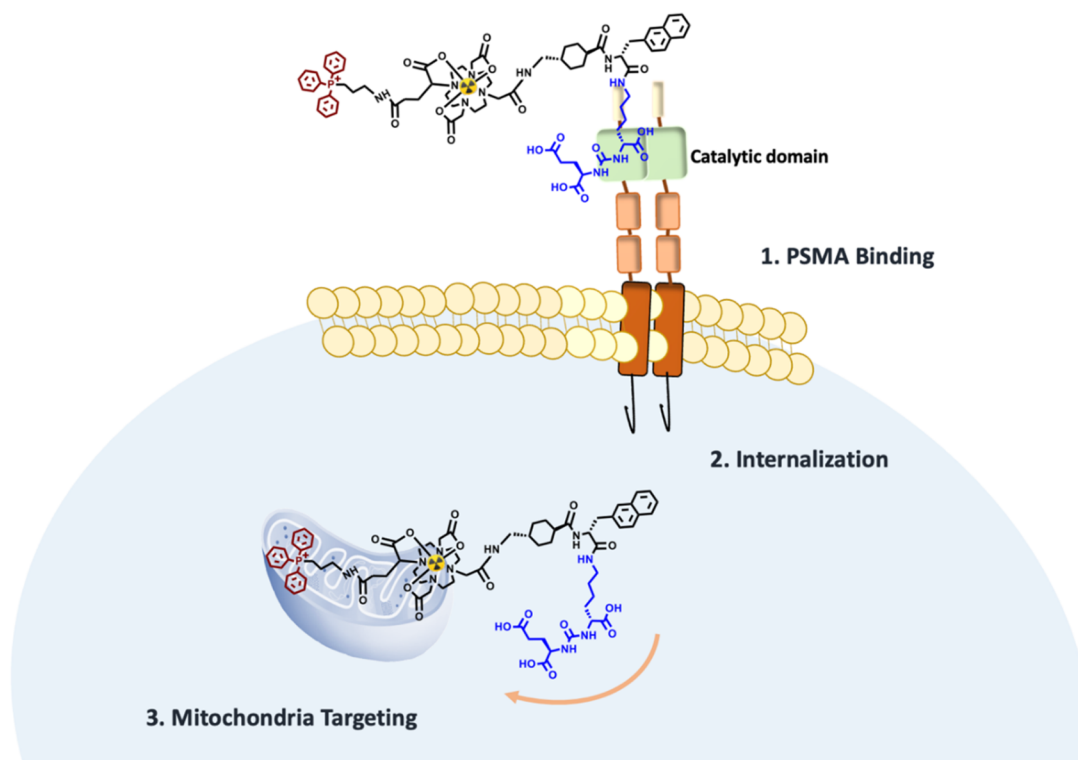
Radiopharmaceuticals offer unique opportunities to explore a theranostic approach of cancer, as one targeting biomolecule recognizing a specific molecular target can be labeled either with diagnostic and/or with therapeutic radionuclides, allowing patient-specific treatments with easier monitoring of the disease progression.<sup>1,2</sup> In the past few years, very encouraging results were obtained for peptides or peptidomimetics radiolabeled with beta emitters, which led to the recent approval of [ $^{177}\text{Lu}$ ]Lu-DOTA-TATE (Lutathera) and [ $^{177}\text{Lu}$ ]Lu-PSMA-617 (Pluvicto) by the FDA and EMA agencies for the treatment of neuroendocrine tumors and prostate cancer (PCa), respectively.<sup>3,4</sup> However, the use of  $\beta^-$  emitters in targeted radionuclide therapy (TRT) of cancer has some limitations, such as the nephrotoxicity and beta radiation resistance encountered in a non-negligible number of patients. Targeted

alpha therapy can be an alternative, and promising preclinical and clinical data were recently reported for different  $^{225}\text{Ac}$ -labeled biomolecules, as for example [ $^{225}\text{Ac}$ ]Ac-PSMA-617.<sup>5</sup> Unfortunately, most alpha emitters have a low availability that limits their clinical use. Auger electron (AE) emitters started to be envisaged as an attractive alternative, since this class of radionuclides has easier availability than alpha emitters and many of them are already commonly used in nuclear medicine imaging (e.g.,  $^{67}\text{Ga}$ ,  $^{99\text{m}}\text{Tc}$ , or  $^{111}\text{In}$ ). In addition, less explored

**Received:** August 28, 2023  
**Revised:** October 31, 2023  
**Accepted:** November 1, 2023  
**Published:** November 22, 2023



a)



b)

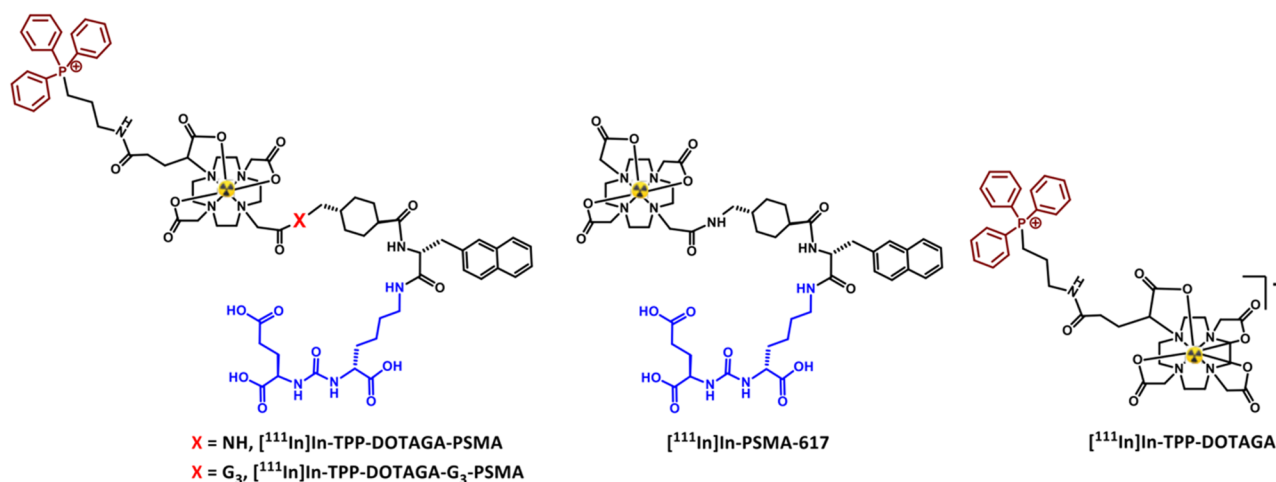


**Figure 1.** a) Schematic drawing of the devised strategy for a cell-specific targeting of the mitochondria of PSMA+ PCa cells. b) Molecular structures of the DOTA-based <sup>111</sup>In-complexes evaluated in this work.

AE emitters with more suitable nuclear properties for TRT are now more available through innovative production methods (e.g., <sup>165</sup>Er, <sup>155</sup>Tb, <sup>161</sup>Tb, <sup>135</sup>La, <sup>195m</sup>Pt, <sup>103m</sup>Rh, <sup>197</sup>Hg, <sup>119</sup>Sb), both for preclinical research and clinical applications.<sup>1,2,6,7</sup>

Most relevantly, Auger electron radiopharmaceutical therapy (AE-RPT) may have the same therapeutic efficacy in oncological small disease compared to  $\alpha$  particle therapy with lower risks of normal tissue toxicity, as the intense shower of low-energy AEs deposits their energy in the immediate vicinity of their site of decay. Despite these potential advantages, clinical trials with AE-emitting radiopharmaceuticals are scarce and are restricted to a few unsuccessful cases using <sup>111</sup>In-labeled peptides and antibodies.<sup>6,8–12</sup> Currently, a <sup>161</sup>Tb-labeled somatostatin antagonist is being evaluated in an ongoing clinical

trial for the TRT of gastroenteropancreatic neuroendocrine tumors (GEP-NET).<sup>13,14</sup> <sup>161</sup>Tb is a  $\beta^-$  emitter but also emits conversion electrons and Auger electrons and thus is expected to allow a combined beta and AE-RPT with an improved therapeutic index.<sup>15,16</sup>

From a dosimetric point of view, the highest relative biological effectiveness (RBE) of AE emitters results when these radionuclides localize in highly radiosensitive organelles (e.g., cellular membrane, nucleus or mitochondria).<sup>17–19</sup> Thus, the design of cancer specific AE-emitting radioconjugates with preferential accumulation in these organelles might lead to better therapeutic outcomes with reduction of undesired side effects (e.g., hematological toxicity, kidney damage, or cardiotoxicity), as enhanced radiotherapeutic effects at lower

doses can be anticipated. However, the design of this type of radioconjugates can be a challenging task due to the impact of the introduction of organelle-specific moieties on their affinity and specificity toward the target cancer cells and also in pharmacokinetics and biodistribution.

In particular, mitochondria-targeted AE-emitting radioconjugates may be an attractive alternative because mitochondrial DNA is damaged by exposure to ionizing radiation and is not so efficiently repaired when compared with nuclear DNA.<sup>20,21</sup> Moreover, the irradiation of the mitochondria can also elicit other deleterious effects such as ROS production or apoptosis.<sup>20,22,23</sup> Having this in mind, we considered the energized mitochondria of tumor cells as a pertinent subcellular target for therapeutic AE-emitting radionuclides. Our initial studies focused on dual-targeted <sup>99m</sup>Tc-radioconjugates of the type TPP-<sup>99m</sup>Tc-BBN, carrying a triphenylphosphonium (TPP) derivative as a mitochondrion-tropic moiety and a bombesin (BBN) peptide for the targeting of PCa cells overexpressing the gastrin releasing peptide receptor (GRPR).<sup>24</sup> <sup>99m</sup>Tc is not an ideal AE emitter for TRT due to its relatively low Auger electron yield but can be considered a readily available “model” radionuclide, useful to “validate” the design of new classes of AE-emitting radioconjugates. The studies with <sup>99m</sup>Tc showed that mitochondria targeting is as effective as the nuclear targeting to induce lethal radiobiological effects in tumor cells.<sup>24,25</sup> Therefore, these results pinpointed that cell-specific mitochondria targeting strategies justify further attention in the design of radioconjugates for AE-RPT of cancer.

Our encouraging results with <sup>99m</sup>Tc prompted us to explore a similar strategy for trivalent AE-emitting radiometals (e.g., <sup>111</sup>In, <sup>161</sup>Tb, or <sup>165</sup>Er), a class of radionuclides with similar radio-pharmaceutical chemistry and offering the opportunity to explore the same bifunctional chelators, namely those based on the 1,4,7,10-tetraazacyclododecane-1,4,7,10-tetraacetic acid (DOTA) framework.<sup>26</sup> We initiated the study with <sup>111</sup>In, due to its easiest accessibility being commercially available. For that, we have designed dual-targeted <sup>111</sup>In-DOTA complexes carrying a PSMA inhibitor and a TPP group to promote a selective uptake by PCa cells overexpressing the prostate specific membrane antigen (PSMA) receptor and radionuclide accumulation in mitochondria, respectively (see Figure 1A).

The design of the dual-targeted conjugates relied on the modification of the PSMA-617 structure used to obtain the clinically approved [<sup>177</sup>Lu]Lu-PSMA-617 (Pluvicto),<sup>4</sup> considering that its biological specificity is rather resilient toward the inclusion of different types of modifiers (e.g., albumin binding domains to slow blood clearance or linkers to tune the hydro/lipophilicity).<sup>27–30</sup> By considering the TPP pharmacophore, we have taken into account our encouraging results with the TPP-<sup>99m</sup>Tc-BBN complexes<sup>24,25</sup> and the large body of evidence supporting the suitability of TPP derivatives as mitochondrion-tropic carriers for drug delivery applications.<sup>31</sup> For example, MitoQ is a molecule combining ubiquinone with TPP, through a decylene chain, used as a mitochondria-targeted antioxidant supplement and undergoing several clinical trials involving patients with different mitochondria-related diseases.<sup>32</sup>

Therefore, in this contribution, we describe two novel multifunctional constructs (TPP-DOTAGA-PSMA and TPP-DOTAGA-G<sub>3</sub>-PSMA) and their respective <sup>nat</sup>In and <sup>111</sup>In-complexes (M-TPP-DOTAGA-PSMA and M-TPP-DOTAGA-G<sub>3</sub>-PSMA, M = <sup>nat</sup>In, <sup>111</sup>In). The new constructs were obtained based on the PSMA-617 framework and carry a TPP group introduced at the pendant carboxylic arm opposed to the

one used to link the Glu-urea-Lys (KuE) PSMA binding motif (Figure 1b). One of these constructs (TPP-DOTAGA-G<sub>3</sub>-PSMA) comprises a GlyGlyGly (G<sub>3</sub>) sequence between the PSMA binding unit and the DOTA framework. The G<sub>3</sub> sequence can act as a cathepsin B cleavable linker, as shown previously by us and other authors.<sup>24,33,34</sup> The intracellular protease cleavage of the linker should release smaller radio-metalated complexes, carrying the TPP mitotropic group, with a possible enhanced ability to target the mitochondria. For comparison purposes, we have also evaluated the single-targeted congeners [<sup>111</sup>In]In-TPP-DOTAGA and [<sup>111</sup>In]In-PSMA-617 functionalized solely with the TPP group and the Glu-urea-Lys PSMA binding motif, respectively (Figure 1b).

Our main goal was to demonstrate that the dual-targeted complexes would retain the specificity and affinity toward the PSMA receptor both *in vitro* in cellular models and *in vivo* in tumor animal models, while leading to stronger radiobiological effects in the target tumor cells when compared with the single-targeted complexes. Toward this goal, as described herein, we have performed several cellular assays for the single- and dual-targeted <sup>111</sup>In-complexes, which included cellular uptake, internalization and PSMA-blocking studies in PCa cell lines (LNCaP, PC3 PIP, and PC3 Flu) with different levels of PSMA expression, subcellular localization experiments and the assessment of radiobiological effects.  $\mu$ SPECT imaging studies in PSMA+ PCa xenografts, performed to evaluate how the different components (TPP and PSMA-617 pharmacophores, cleavable linker) influence the *in vivo* behavior of the radioconjugates, are also presented.

## 2. METHODS

**2.1. Materials and General Procedures.** Unless otherwise stated, all chemicals and solvents were reagent grade and used without further purification. The macrocycle derivatives DOTA-GA(tBu)<sub>4</sub> (**1**) ((R)-5-(*tert*-butoxy)-5-oxo-4-(4,7,10-tris(2-(*tert*-butoxy)-2-oxoethyl)-1,4,7,10-tetraazacyclododecan-1-yl)-pentanoic acid) and PSMA-617 were purchased from Chematech (Dijon, France) and Pepmic (Suzhou, Jiangsu, China), respectively. Fmoc-chloride and human serum were purchased from Sigma-Aldrich. (3-Aminopropyl)-triphenylphosphonium bromide (**2**) and the DOTA prochelator (2-[4,10-bis(2-*tert*-butoxy-2-oxo-ethyl)-7-(2-ethoxy-2-oxo-ethyl)-1,4,7,10-tetraazacyclododec-1-yl]acetic acid) (**4**) were synthesized as we have described elsewhere.<sup>24,35</sup> InCl<sub>3</sub> (anhydrous 99%) was acquired from Alfa Aesar (Germany). [<sup>111</sup>In]InCl<sub>3</sub> (370 MBq/mL in HCl) was obtained from Mallinckrodt (Curium) Medical B.V. (Netherlands).

<sup>1</sup>H, <sup>13</sup>C, and <sup>31</sup>P NMR spectra were recorded on a Bruker Avance III 300 MHz spectrometer. The chemical shifts ( $\delta$ ) are given in ppm and were referenced to the residual solvent resonances relative to tetramethylsilane (SiMe<sub>4</sub>), and the <sup>31</sup>P chemical shifts were referenced with external 85% H<sub>3</sub>PO<sub>4</sub> solution. Coupling constants (*J*) are given in Hz.

Mass spectra were acquired in an electrospray ionization/quadrupole ion trap (ESI/QITMS) Bruker HCT mass spectrometer. Samples were injected in mixtures of water:acetonitrile (ACN) or water:methanol (MeOH) and injected at a flow rate of 150  $\mu$ L.h<sup>-1</sup>.

Column chromatography was performed with silica gel 60 (Merck). HPLC analysis and purification of the chelators, <sup>nat</sup>In complexes, and <sup>111</sup>In-complexes was performed on four different systems with different elution methods, as described below.

**2.1.1. System I.** PerkinElmer Series 200 analytical HPLC instrument, equipped with a UV–vis detector (LC 290), with a Supelco Analytical Discovery BIO WidePore C18\_5 column (250 mm × 4.6 mm, 300 Å pore size, 5 μm particle size) with a flow rate of 1 mL/min. HPLC solvents consisted of 0.1% trifluoroacetic acid (TFA) in water (eluent A) and 0.1% TFA in ACN (eluent B). **Method A** (gradient): 100% A to 100% B in 15 min, 100% B 5 min, 100% B to 100% A in 1 min, and 100% A 4 min. **Method B** (gradient): 95% A/5% B to 100% B in 25 min, 100% B 2 min, 100% B to 95% A/5% B in 1 min, 95% A/5% B 2 min.

**2.1.2. System II.** Waters semipreparative HPLC instrument (Waters 2535 Quaternary Gradient Module), equipped with a diode array detector (Waters 2996) with a VP 250/8 Nucleosil 100–7 C18 column (250 × 8 mm, 100 Å pore size, 7 μm particle size) with a flow rate of 2 mL/min. HPLC solvents consisted of 0.1% TFA in water (eluent A) and 0.1% TFA in ACN (eluent B). **Method C** (gradient): 95% A/5% B to 100% B in 25 min, 100% B in 5 min, 100% B to 95% A/5% B in 2 min, 95% A/5% B in 8 min.

**2.1.3. System III.** PerkinElmer Flexar analytical HPLC coupled to a PerkinElmer Flexar UV/vis Detector and to a Lablogic Flow-RAM gamma detector with a EC 250/4 Nucleosil (Macherey-Nagel) 100–10 C18 column (REF 720023.40–250 × 4 mm, 300 Å pore size, 5 μm particle size) with a flow rate of 1 mL/min. HPLC solvents consisted of 0.1% TFA in water (eluent A) and 0.1% TFA in ACN (eluent B). Both UV absorbance and γ radiation were monitored. **Method D** (gradient): same gradient as in Method B.

**2.1.4. System IV.** PerkinElmer LC 200 analytical HPLC coupled to a LC 290 UV/vis Detector and to a Berthold LB-507A radiometric detector with a EC 250/4 Nucleosil (Macherey-Nagel) 100–10 C18 column (REF 720023.40–250 × 4 mm, 300 Å pore size, 5 μm particle size) with a flow rate of 1 mL/min. HPLC solvents consisted of 0.1% TFA in water (eluent A) and 0.1% TFA in ACN (eluent B). Both UV absorbance and γ radiation were monitored. **Method E** (gradient): same gradient as in Method B.

## 2.2. Synthesis of the TPP-Containing Chelators.

**2.2.1. (3-(5-(tert-Butoxy)-5-oxo-4-(4,7,10-tris(2-(tert-butoxy)-2-oxoethyl)-1,4,7,10-tetraazacyclododecan-1-yl)-pentanamido)propyl)triphenylphosphonium Bromide (3).** A solution of compound 2 (96.0 mg, 0.3 mmol) in dry dimethylformamide (DMF) (5 mL) and *N,N*-diisopropylethylamine (DIPEA) (100 μL, 0.58 mmol) was stirred for 20 min. In a separate flask, 2-(1*H*-benzotriazole-1-yl)-1,1,3,3-tetramethyluronium hexafluorophosphate (HBTU) (83.4 mg, 0.22 mmol) and DIPEA (76.6 μL, 0.44 mmol) were added to a solution of compound 1 (140.0 mg, 0.2 mmol) in dry DMF (5 mL) and stirred for 20 min, and then this solution was added to the first solution. The mixture was stirred overnight and monitored by HPLC (Method A) to verify the reaction progress. After the evaporation of the solvents in a vacuum line, the crude was dissolved in CHCl<sub>3</sub> and extracted 3 times with water. The combined organic phases were dried with MgSO<sub>4</sub> and filtered, and the filtrate was evaporated to dryness under vacuum to afford 3 as a white solid (270.0 mg, 90%). ESI(+)-MS *m/z* calcd for [C<sub>56</sub>H<sub>85</sub>N<sub>5</sub>O<sub>9</sub>P]<sup>+</sup>: 1002.61, found: 1002.7 [M]<sup>+</sup>.

**2.2.2. (3-(4-Carboxy-4-(4,7,10-tris(carboxymethyl)-1,4,7,10-tetraazacyclododecan-1-yl)butanamido)propyl)triphenylphosphonium Bromide (TPP-DOTAGA).** To compound 3 (230.0 mg, 0.2 mmol) was added 4 mL of TFA/dichloromethane (DCM) (1:1). The reaction mixture was stirred overnight and monitored by HPLC (Method A) to verify

the reaction progress. After removal of the volatiles, the product was purified using a Sep-Pak C18 cartridge using water with 0.1% TFA and increasing concentrations of ACN with 0.05% TFA. The product was eluted with 20% of ACN with 0.1% TFA and lyophilized to afford TPP-DOTAGA as a white solid (120.0 mg, 67%). <sup>1</sup>H NMR (300 MHz, CD<sub>3</sub>OD) δ 7.89–7.77 (m, 15H, CH, Ar-PPh<sub>3</sub>), 4.11–3.91 (m, 4H, CH<sub>2</sub>), 3.64–3.08 (m, 23H, CH<sub>2</sub>COOH, NCH<sub>2</sub>CH<sub>2</sub>N, NCH), 2.52 (m, 2H, CH<sub>2</sub>), 1.97–1.86 (m, 4H, CH<sub>2</sub>); <sup>31</sup>P NMR (MHz, CD<sub>3</sub>OD) δ 24.07. ESI(+)-MS *m/z* calcd for [C<sub>40</sub>H<sub>53</sub>N<sub>5</sub>O<sub>9</sub>P]<sup>+</sup>: 778.36, found: 778.3 [M]<sup>+</sup>; calcd for [M + H]<sup>2+</sup>: 389.68, found: 389.7 [M + H]<sup>2+</sup>.

**2.2.3. (3-(4-(4,10-Bis(2-(tert-butoxy)-2-oxoethyl)-7-(2-ethoxy-2-oxoethyl)-1,4,7,10-tetraazacyclododecan-1-yl)-5-(tert-butoxy)-5-oxopentanamido)propyl)triphenylphosphonium Bromide (5).** A solution of compound 2 (96.0 mg, 0.3 mmol) in dry DMF (5 mL) and DIPEA (100 μL, 0.58 mmol) was stirred for 1 h. In a separate flask, HBTU (135.4 mg, 0.36 mmol) and DIPEA (176.6 μL, 1.01 mmol) were added to a solution of compound 4 (130 mg, 0.19 mmol) in dry DMF (5 mL). The activation reaction proceeded for 10 min, and the solution containing activated compound 4 was added to the compound 2 solution. The mixture was stirred overnight and monitored by HPLC (Method A). After removal of the volatiles, the crude product was dissolved in CHCl<sub>3</sub> and extracted 3 times with water. The organic phase was concentrated under a vacuum and further purified by column chromatography on silica gel (95% DCM, 5% MeOH), affording compound 5 as a yellow oil (137 mg, 74%). ESI(+)-MS *m/z* calcd for [C<sub>54</sub>H<sub>81</sub>N<sub>5</sub>O<sub>9</sub>P]<sup>+</sup>: 974.58, found: 974.6 [M]<sup>+</sup>.

**2.2.4. (3-(4-(4,10-Bis(2-(tert-butoxy)-2-oxoethyl)-7-(carboxymethyl)-1,4,7,10-tetraazacyclododecan-1-yl)-5-(tert-butoxy)-5-oxopentanamido)propyl)triphenylphosphonium Bromide (6).** Compound 5 (137 mg, 0.14 mmol) was dissolved in a solution of NaOH (24.0 mg, 0.6 mmol) in water (2 mL). The mixture was stirred for 6 h, and the progress of the hydrolysis reaction was monitored by HPLC (Method A). After the reaction was completed, the mixture was neutralized with 3 M HCl (160 μL), and the product was extracted from water to CHCl<sub>3</sub> (3×). The combined organic phases were concentrated under vacuum, and the crude was further purified using a Sep-Pak C18 cartridge eluted with a mixture of 0.1% TFA in water and 0.05% TFA in ACN, with a stepwise increasing percentage of the organic solution during the elution. The collected fractions were lyophilized to afford compound 6 as a white solid (94.7 mg, 71%). <sup>1</sup>H NMR (300 MHz, CD<sub>3</sub>OD) δ 7.97–7.81 (m, 15H, CH, Ar-PPh<sub>3</sub>), 4.2–1.9 (m, 33H, COONCH<sub>2</sub>CH<sub>2</sub>, NCH<sub>2</sub>, CH<sub>2</sub>COOH, NCH<sub>2</sub>COO(CH<sub>3</sub>)<sub>3</sub>), NCH, NCHCH<sub>2</sub>CH<sub>2</sub>), 1.57 (m, 27H, C(CH<sub>3</sub>)<sub>3</sub>). <sup>13</sup>C NMR (100 MHz, CD<sub>3</sub>OD) δ 163.25, 162.83, 162.56, 162.17, 136.43, 136.40, 134.85, 134.75, 131.66, 131.54, 120.10, 119.68, 119.24, 116.73, 113.82, 55.74, 48.45, 40.60, 40.41, 28.75, 28.46, 23.73, 21.74, 21.03, 20.46. <sup>31</sup>P NMR (MHz, CD<sub>3</sub>OD) δ 23.64. ESI(+)-MS *m/z* calcd for [C<sub>52</sub>H<sub>77</sub>N<sub>5</sub>O<sub>9</sub>P]<sup>+</sup>: 946.54, found: 946.5 [M]<sup>+</sup>; calcd for [M + H]<sup>2+</sup>: 473.78, found: 473.9.

### 2.2.5. Synthesis of Protected Dual-Targeted Precursors.

**2.2.5.1. General Procedure.** The <sup>t</sup>OBu-protected PSMA derivatives, compounds 9 (0.012 mmol) and 10 (0.010 mmol) (synthesized as described in the Supporting Information), were reacted with 1.2 equiv of compound 6 dissolved in dry DMF (3 mL), in the presence of 1.2 equiv of HBTU and 4 equiv of DIPEA. The activation reaction of 6 proceeded for 10 min, prior to the addition of compounds 9 and 10 in dry DMF (3 mL). The mixture was stirred for 2 h, and the progress of

reaction was monitored by HPLC to follow the formation of TPP-DOTAGA-(tBu)<sub>3</sub>-PSMA-(tBu)<sub>3</sub> (**12**) and TPP-DOTAGA-(tBu)<sub>3</sub>-G<sub>3</sub>-PSMA-(tBu)<sub>3</sub> (**13**), respectively. The volatiles were removed and the crude was purified using a Sep-Pak C18 cartridge eluted with a mixture of 0.1% TFA in water and 0.1% TFA in ACN, with a stepwise increasing percentage of the organic solution during the elution. The fractions containing the product were combined and lyophilized affording the desired compounds as white powders.

**2.2.5.2. TPP-DOTAGA-(tBu)<sub>3</sub>-PSMA-(tBu)<sub>3</sub> (**11**).** Yield: 9.6 mg, 45%; HPLC (Method B): Rt = 23.8 min; ESI(+)-MS *m/z* calcd for [C<sub>97</sub>H<sub>144</sub>N<sub>10</sub>O<sub>17</sub>P]<sup>+</sup>: 1752.04; calcd for [M + H]<sup>2+</sup>: 877.02, found: 877.1 [M + H]<sup>2+</sup>.

**2.2.5.3. TPP-DOTAGA-(tBu)<sub>3</sub>-G<sub>3</sub>-PSMA-(tBu)<sub>3</sub> (**12**).** Yield: 8.3 mg, 43%; HPLC (Method B): Rt = 20.5 min; ESI(+)-MS *m/z* calcd [C<sub>103</sub>H<sub>153</sub>N<sub>13</sub>O<sub>20</sub>P]<sup>+</sup>: 1923.11; calcd for [M + H]<sup>2+</sup>: 962.56, found: 962.9 [M + H]<sup>2+</sup>.

**2.2.6. Synthesis of Dual-Targeted Chelators.** **2.2.6.1. General Procedure.** The compounds TPP-DOTAGA-(tBu)<sub>3</sub>-PSMA-(tBu)<sub>3</sub> (**11**) and TPP-DOTAGA-(tBu)<sub>3</sub>-G<sub>3</sub>-PSMA-(tBu)<sub>3</sub> (**12**) were dissolved in 2 mL of a mixture of trifluoroacetic acid (TFA), triisopropylsilane (TIPS), and water (95:2.5:2.5), and each reaction mixture was stirred overnight. After this time, the reaction progress was monitored by HPLC and then the volatiles were removed under vacuum. The crude was redissolved in a mixture of ACN and water (1:1) and purified by HPLC (Method B). The collected fractions were lyophilized to afford TPP-DOTAGA-PSMA or TPP-DOTAGA-G<sub>3</sub>-PSMA as white solids.

**2.2.6.2. TPP-DOTAGA-PSMA.** Yield: 4.9 mg, 63%; HPLC (Method B): Rt = 14.0 min; ESI(+)-MS *m/z* calcd for [C<sub>73</sub>H<sub>96</sub>N<sub>10</sub>O<sub>17</sub>P]<sup>+</sup>: 1415.67, found: 1415.7 [M]<sup>+</sup>; calcd for [M + H]<sup>2+</sup>: 708.33, found 708.5 [M + H]<sup>2+</sup>.

**2.2.6.3. TPP-DOTAGA-G<sub>3</sub>-PSMA.** Yield: 4.0 mg, 58%; HPLC (Method B): Rt = 14.2 min; ESI(+)-MS *m/z* calcd [C<sub>79</sub>H<sub>105</sub>N<sub>13</sub>O<sub>20</sub>P]<sup>+</sup>: 1586.73; calcd for [M + H]<sup>2+</sup>: 793.87, found: 794.1 [M + H]<sup>2+</sup>.

**2.3. Synthesis of the Complexes with <sup>nat</sup>In.** **2.3.1. General Procedure.** Always using sodium acetate buffer (0.1 M, pH 5) as the solvent, 50 μL of a 1 mg/mL solution of each ligand (TPP-DOTAGA, PSMA-617, TPP-DOTAGA-PSMA, or TPP-DOTAGA-G<sub>3</sub>-PSMA) were added to the appropriate volume of a <sup>nat</sup>InCl<sub>3</sub> solution (10 mg/mL) corresponding to a 5:1 molar ratio <sup>nat</sup>InCl<sub>3</sub>/ligand. Then, the total volume was adjusted to 500 μL, and the final solution was heated at 95 °C for 30 min. After cooling, the mixture was purified using a Sep-Pak Light C18 cartridge that was eluted with 0.5 mL of 0.05% TFA in ACN to recover the different <sup>nat</sup>In complexes, which were obtained in a quantitative way after removal of the solvent under vacuum.

**2.3.2. <sup>nat</sup>In-TPP-DOTAGA.** HPLC (Method E, UV detection): Rt = 15.2 min. ESI(+)-MS *m/z* calcd for [C<sub>40</sub>H<sub>50</sub>N<sub>5</sub>O<sub>9</sub>InP]<sup>+</sup>: 890.24, found: 890.4 [M]<sup>+</sup>; calcd for [M + H]<sup>2+</sup>: 445.62, found: 445.7 [M + H]<sup>2+</sup>.

**2.3.3. <sup>nat</sup>In-PSMA-617.** HPLC (Method E, UV detection): Rt = 13.7 min. ESI(+)-MS *m/z* calcd for C<sub>49</sub>H<sub>68</sub>N<sub>9</sub>O<sub>16</sub>In: 1153.38, found: 1154.4 [M + H]<sup>+</sup>; calcd for [M+2H]<sup>2+</sup>: 577.70, found: 577.8 [M+2H]<sup>2+</sup>.

**2.3.4. <sup>nat</sup>In-TPP-DOTAGA-PSMA.** HPLC (Method D, UV detection): Rt = 14.6 min. ESI(+)-MS *m/z* calcd for [C<sub>73</sub>H<sub>93</sub>N<sub>10</sub>O<sub>17</sub>InP]<sup>+</sup>: 1527.55, found: 1527.6 [M]<sup>+</sup>; calcd for [M + H]<sup>2+</sup>: 764.28, found: 764.6 [M + H]<sup>2+</sup>.

**2.3.5. <sup>nat</sup>In-TPP-DOTAGA-G<sub>3</sub>-PSMA.** HPLC (Method D, UV detection): Rt = 14.2 min. ESI(+)-MS *m/z* calcd for [C<sub>79</sub>H<sub>102</sub>N<sub>13</sub>O<sub>20</sub>InP]<sup>+</sup>: 1698.61; calcd for [M + H]<sup>2+</sup>: 849.81, found: 850.2 [M + H]<sup>2+</sup>.

**2.4. Synthesis of the <sup>111</sup>In Radiocomplexes.** **2.4.1. General Procedure.** 5–40 μL of <sup>111</sup>InCl<sub>3</sub> (3.7 to 40.8 MBq) were added to 2.5 nmol of each ligand (TPP-DOTAGA, PSMA-617, TPP-DOTAGA-PSMA, and TPP-DOTAGA-G<sub>3</sub>-PSMA) dissolved at a 1 mg/mL concentration in sodium acetate buffer (0.1 M, pH 5). Then, the appropriate volume of sodium acetate buffer (0.1 M, pH 5) was added to the radiolabeling mixture until a total volume of 250 μL, corresponding to a final ligand concentration of 10 μM. Thereafter, the solution was heated at 95 °C for 15 min. After cooling, the mixture was applied in a Sep-Pak Light C18 cartridge, and the radiocomplexes were eluted with 1 mL of EtOH with 0.05% TFA. The radiocomplexes fraction was added to 100 μL of a freshly prepared PBS solution containing sodium ascorbate pH 7 (5 mg/mL), and the organic solvent was evaporated under a N<sub>2</sub> stream at room temperature. The radiochemical yield (RCY) and radiochemical purity (RCP) were determined by HPLC (Method D, γ detection).

**2.4.2. [<sup>111</sup>In]In-TPP-DOTAGA.** HPLC (Method E, γ detection): Rt = 15.4 min. RCY > 95%. RCP > 98%.

**2.4.3. [<sup>111</sup>In]In-PSMA-617.** HPLC (Method E, γ detection): Rt = 13.9 min. RCY > 95%. RCP > 98%.

**2.4.4. [<sup>111</sup>In]In-TPP-DOTAGA-PSMA.** HPLC (Method D, γ detection): Rt = 14.7 min. RCY > 95%. RCP > 98%.

**2.4.5. [<sup>111</sup>In]In-TPP-DOTAGA-G<sub>3</sub>-PSMA.** HPLC (Method D, γ detection): Rt = 14.4 min. RCY > 95%. RCP > 98%.

**2.5. In Vitro Evaluation Studies.** **2.5.1. Radiochemical Stability.** The *in vitro* stability of the <sup>111</sup>In-radiocomplexes was studied by HPLC analysis of the radiolabeled compound (typically 1–5 MBq) dissolved in different media. The evaluation of the radiochemical stability was carried out in PBS and cell culture medium (RPMI 1640). A suitable volume of the radioactive complexes was diluted into 4 times the volume of the cell medium; the mixtures were incubated at 37 °C and aliquots were taken at the different time points and analyzed by radioHPLC.

**2.5.2. Lipophilicity Determination.** The octanol–water partition coefficients (*P*<sub>o/w</sub>) of the <sup>111</sup>In-radiocomplexes were determined by the “shake-flask” method.<sup>36</sup> The radiolabeled conjugates (20 μL, typically 1 to 5 MBq) were added to a mixture of PBS (pH 7.4, 1 mL) and 1-octanol (1 mL) previously saturated in each other by vigorous stirring. The mixture was vortexed and centrifuged (3000 rpm, 10 min, RT) to allow for phase separation. After phase separation, aliquots (100 μL) of both organic and water phases were measured in a gamma counter and the ratio between the radioactivity in both phases was calculated and results expressed as log *D*<sub>pH7.4</sub>.

**2.6. Cellular Studies.** **2.6.1. Cell Culture.** The LNCaP prostate cancer cell line was kindly provided by the Portuguese Institute of Oncology (Porto, Portugal). Sublines of the androgen-independent PC3 human prostate cancer cell line, PSMA-positive (PSMA+) PC3 PIP and PSMA-negative (PSMA–) PC3 flu cells, were kindly provided by Prof. Dr. Martin Pomper (Johns Hopkins University School of Medicine, Baltimore, MD, USA).<sup>37</sup> The LNCaP cells were cultured in an RPMI 1640 containing 10% fetal bovine serum (FBS). PC3 PIP and PC3 flu cells were grown under the same culture medium but supplemented with 0.02% puromycin antibiotic to maintain PSMA expression in the PSMA+ cell line. All cell culture reagents were purchased from Gibco (Thermo Fisher Scientific,

Waltham, MA, USA). All cell cultures were maintained in an atmosphere of 5% carbon dioxide (CO<sub>2</sub>) at 37.0 °C in a humidified incubator (Heraeus, Hanau, Germany) and tested for mycoplasma using the LookOut mycoplasma PCR Detection kit.

**2.6.2. Competitive Binding Assay.** The *in vitro* cell-binding assays were performed in PC3 PIP cells. Briefly, cells were seeded in 24-well plates (150,000 cells per well) and allowed to attach overnight. Competition was conducted by incubation of HPLC purified [<sup>111</sup>In]In-PSMA-617 (50,000 cpm in 0.2 mL) in the presence of increasing concentrations (10<sup>-12</sup>–10<sup>-5</sup> M) of the PSMA-containing DOTA chelators and respective In complexes (<sup>nat</sup>In-TPP-DOTAGA-PSMA, <sup>nat</sup>In-TPP-DOTAGA-G<sub>3</sub>-PSMA, <sup>nat</sup>In-PSMA-617) in binding assay medium (RPMI 1640 supplemented with 1% (v/v) FBS and 25 mM HEPES, 0.1 mL, total volume per well 0.3 mL) for 90 min at room temperature. The binding was interrupted by removing the medium and washing the cells twice with ice-cold PBS. Cells were then lysed with 1 M NaOH treatment (2 × 0.4 mL, 10 min at 37 °C). Lysates were collected and counted for their radioactivity content in an automated  $\gamma$  counter (HIDEX AMG, Hidex, Turku, Finland). IC<sub>50</sub> values (concentration of competitor required to inhibit 50% of the maximum radioligand binding) were calculated by nonlinear regression according to a one-site model using GraphPad Prism 8.0 software (San Diego, CA, USA) and are represented as the average of two independent experiments.

**2.6.3. Cellular Uptake and Internalization.** Time-dependent accumulation of <sup>111</sup>In-complexes in tumor cells was studied by using PSMA-positive LNCaP and PC3 PIP and PSMA-negative PC3 flu cell lines. The expression level of the PSMA protein in these different cell lines was confirmed by Western blot analysis (Supporting Information). Cells were seeded at a density of 0.2 million (LNCaP) or 0.15 million (PC3 PIP and PC3 flu) per well in 24 well-plates and allowed to attach overnight. Then, cells were incubated at 37 °C for a period of 5 min to 4 h with about 7.4 kBq (0.2  $\mu$ Ci) of the radiocomplex in 0.5 mL of assay medium (RPMI 1640 containing 10% FBS and 1% penicillin–streptomycin). After each incubation time, the unbound radiocomplex was removed and the cells washed with ice-cold RPMI medium. Cell surface-bound radiocomplex was removed by two steps of acid wash (50 mM glycine-HCl/100 mM NaCl buffer, pH 2.8) at room temperature for 4 min. The pH was neutralized with PBS, and subsequently the cells were lysed with 1 M NaOH for 10 min at 37 °C to determine internalized radiocomplex. The activity in both cell surface-bound and internalized fractions was measured using a gamma counter (HIDEX AMG, Hidex, Turku, Finland) and is reported as a proportion to the total applied radioactivity. Each assay was performed in quadruplicate and data are presented as mean  $\pm$  SEM of typically three independent experiments. For assessing the specific PSMA-mediated cellular uptake and internalization of [<sup>111</sup>In]In-TPP-DOTAGA-PSMA, [<sup>111</sup>In]In-TPP-DOTAGA-G<sub>3</sub>-PSMA, and [<sup>111</sup>In]In-PSMA-617, a similar study was performed in PC3 PIP cells in which these radiocomplexes were incubated for 0.5, 1, and 3 h with or without the PSMA inhibitor 2-(phosphonomethyl)pentanedioic acid (2-PMPA, Sigma) (100  $\mu$ M/0.5 mL/well).

**2.6.4. Nuclear Uptake.** PC3 PIP cells were seeded at a density of 0.6 million per well in 6 well-plates and allowed to attach for 2 days. The cells were incubated with 37 kBq (1  $\mu$ Ci)/well of [<sup>111</sup>In]In-TPP-DOTAGA-PSMA, [<sup>111</sup>In]In-TPP-DOTAGA-G<sub>3</sub>-PSMA, and [<sup>111</sup>In]In-PSMA-617 in 1.5 mL of culture

medium, for 30, 60, 90, 120, and 180 min, at 37 °C. At each time point, cells in radioactive media were removed from the plates by scrapping and collected into a 2 mL tube. The unbound radioactive complex was removed by centrifugation of the cell suspension at 4 °C, followed by washing the cellular pellet with ice-cold PBS. The pellet was then resuspended in 1.9 mL of ice-cold cell lysis buffer (10 mM Tris, 1.5 mM MgCl<sub>2</sub>, and 140 mM NaCl) containing 0.1% of IGEPAL-ca. 630 (Sigma) and incubated on ice for 10 min to disrupt the cell membrane. After the lysis, the suspension was centrifuged at 1300 × g for 2 min at 4 °C, the supernatant (cytoplasm) was separated from the pellet (nuclei), and the activity in both fractions measured. The nuclear uptake was expressed as a percentage of applied activity and, typically, was determined based on three independent experiments.

**2.6.5. Mitochondrial Uptake.** Adherent and confluent PC3 PIP cells (T75 culture flask) were incubated with about 3.7 MBq (100  $\mu$ Ci) of the radiocomplex ([<sup>111</sup>In]In-PSMA-617, [<sup>111</sup>In]In-TPP-DOTAGA-PSMA, or [<sup>111</sup>In]In-TPP-DOTAGA-G<sub>3</sub>-PSMA) in 4 mL of culture medium (RPMI) for 1 h and 2 h at 37 °C and 5% CO<sub>2</sub>. Cells were collected by scraping, and the harvested cell suspension was centrifuged at 850 × g for 2 min at 4 °C. The cell pellet was washed with cold PBS to remove the unbound radiocomplex, and the activity of whole-cell fraction was measured (cellular uptake determination). To obtain the mitochondrial fraction, cells were treated with the “Mitochondria Isolation Kit, human” (Miltenyi Biotec), according to the manufacturer’s protocol. Briefly, the pellet was resuspended with ice-cold lysis buffer (1.5 mL/1 × 10<sup>7</sup> cells) supplemented with a cocktail of protease inhibitors, and the cells were homogenized using a needle. Then, 1× separation buffer was added to obtain 10 mL of solution, and a 50  $\mu$ L aliquot of Anti-TOM22 MicroBeads was added to magnetically label the mitochondria. The mixture was incubated for 1 h in the refrigerator with gentle shaking using a rotator. Afterward, a LS Column was placed in the magnetic field of a MACS Separator and was rinsed with 3 mL of 1× separation buffer. The cell lysate was applied into the column stepwise (3 × 3.3 mL) to obtain the flow-through. Then, the column was washed with 3 × 3 mL of 1× separation buffer, removed from the separator and 1.5 mL of 1× separation buffer was added to the column and the magnetically labeled mitochondria were eluted immediately with the plunger. The final fractions were measured in an automated  $\gamma$ -counter (HIDEX AMG, Hidex, Turku, Finland). Data are represented as the average of two independent experiments.

**2.6.6. Clonogenic Assay.** *In vitro* cell survival was tested by using the clonogenic survival assay. Cells (200–400) were seeded in 6 well-plates and allowed to attach overnight. Radiolabeled complexes at different activities (0, 5, 10, 20, 50, and 75  $\mu$ Ci; 0.185–2.775 MBq/1.5 mL) were diluted in prewarmed culture medium and incubated with the cells for 24 h at 37 °C. Then, the medium with the radiolabeled compound was removed, and cells were washed with PBS and left to grow with fresh medium for 10 days or until colonies had at least 50 cells. Colonies were fixed with methanol/glacial acetic acid (3:1) and stained with Giemsa (4%). The plating efficiency (PE), ratio of the number of colonies to the number of cells seeded, and the survival fraction (SF, number of colonies after treatment, expressed in terms of PE) were obtained following the methodology described in literature,<sup>38</sup> where

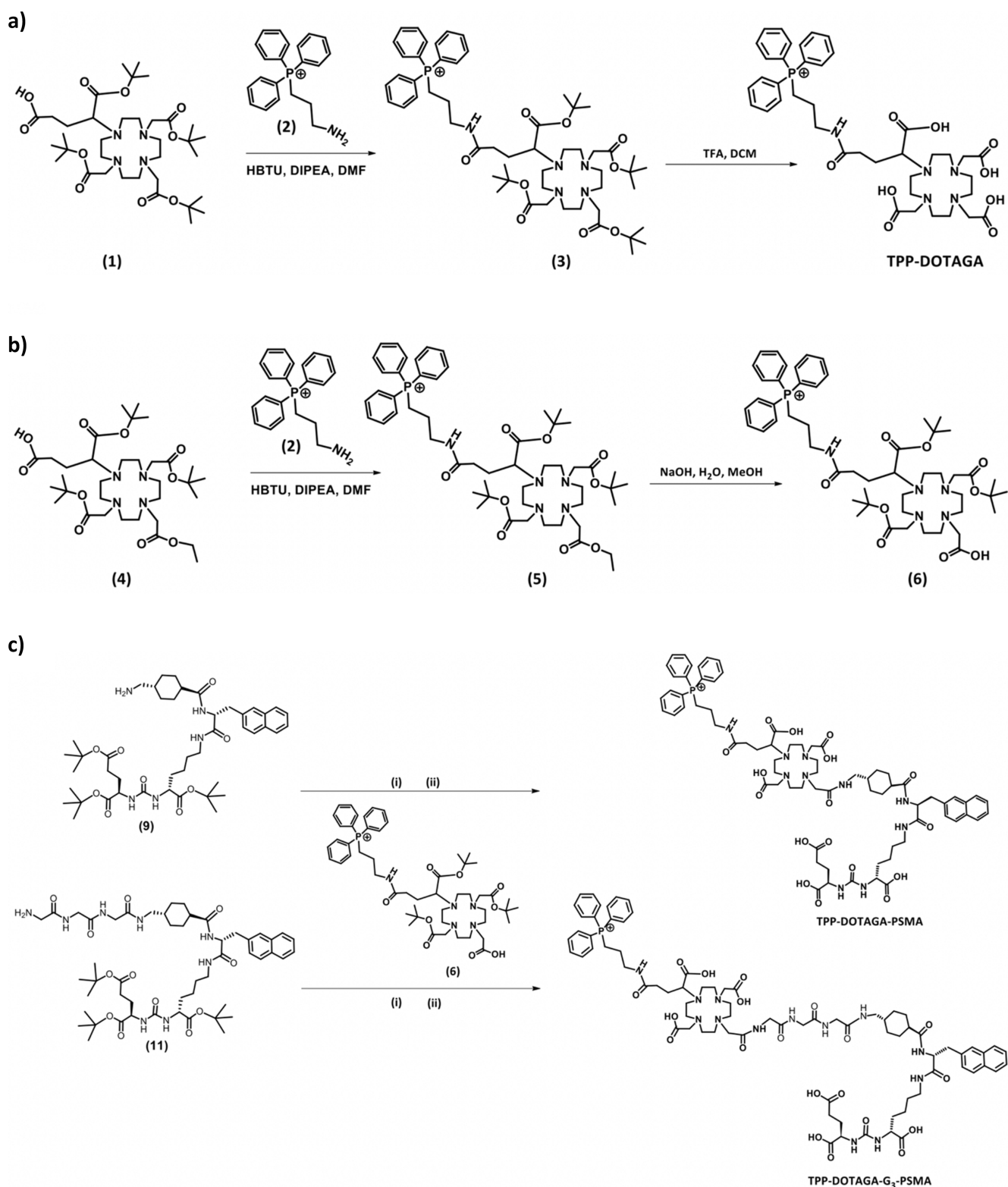


**Figure 2.** Chemical synthesis of the TPP-containing chelators and their precursors: a) single-targeted chelator **TPP-DOTAGA**; b) DOTA prochelator (6) bearing orthogonal protecting groups used to obtain the TPP-containing dual-targeted chelators; and c) dual-targeted chelators **TPP-DOTAGA-PSMA** and **TPP-DOTAGA-G<sub>3</sub>-PSMA**. (i) HBTU, DIPEA, and DMF; (ii) TFA/TIS/H<sub>2</sub>O (95:2.5:2.5).

$$PE = \frac{\text{number of colonies formed}}{\text{number of cells seeded}} \times 100\% \quad (1)$$

$$SF = \frac{\text{number of colonies formed after treatment}}{\text{number of cells seeded} \times PE} \quad (2)$$

**2.7. In Vivo Studies.** Animals were kept in individually ventilated cages in a temperature-controlled (approximately 22 °C) and humidity-controlled facility with a 12 h–12 h light-dark cycle and unlimited access to food and water. All animal procedures were approved by the KU Leuven ethical review

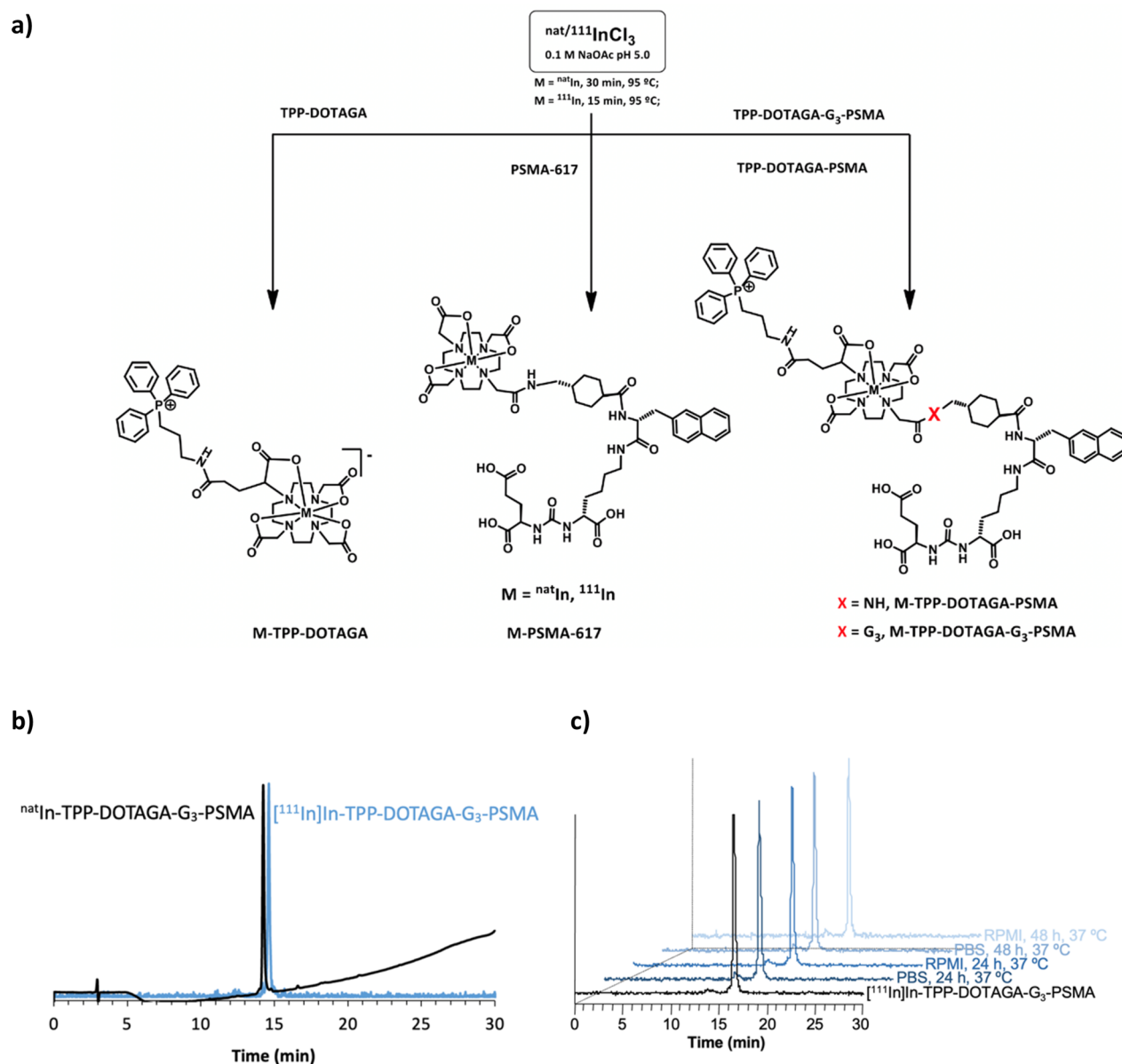


**Figure 3.** Preparation and characterization of the In complexes and *in vitro* stability studies: a) Synthesis of the <sup>nat</sup>In and <sup>111</sup>In complexes; b) HPLC chromatogram of <sup>nat</sup>In-TPP-DOTAGA-G<sub>3</sub>-PSMA (UV detection, 220 nm) and [<sup>111</sup>In]In-TPP-DOTAGA-G<sub>3</sub>-PSMA ( $\gamma$  detection); c) RP-HPLC radiochromatograms ( $\gamma$ -detection) of [<sup>111</sup>In]In-TPP-DOTAGA-G<sub>3</sub>-PSMA after incubation in PBS pH 7.4 and RPMI cell culture at 37 °C for 24 and 48 h.

board (ethical approval reference P200/2021) and were carried out in accordance with Directive 2010/63/EU. Female SCID/Beige mice (Charles River, Brussels, Belgium) were selected and xenografted with two different tumor cell lines: PSMA-negative PC3 cells (PC3-Flu) and PSMA-positive PC3 cells (PC3-PIP). Six-week-old mice were injected subcutaneously with 1.0–1.1 million cells (RPMI medium with Cultrex, 1:1, Bio-Techne, Dublin, Ireland) in the left and right shoulder region with PC3-Flu and PC3-PIP cells, respectively.

Xenografted mice were injected with a freshly filtered (0.22  $\mu$ m, Millipore) bolus of  $\sim$ 25 MBq, 1–2 nmol of either [<sup>111</sup>In]In-PSMA-617, [<sup>111</sup>In]In-TPP-DOTAGA-PSMA, [<sup>111</sup>In]In-TPP-DOTAGA-G<sub>3</sub>-PSMA, or [<sup>111</sup>In]In-TPP-DOTAGA, which was administered via tail vein injection.

**2.7.1.  $\mu$ SPECT Imaging.** For *in vivo*  $\mu$ SPECT imaging, anesthesia was induced using 5% isoflurane in a constant flow of

oxygen at 1 L/min, after which the isoflurane concentration was reduced to 2% during imaging. Vital signs of the mice were continuously monitored during both SPECT and CT scanning procedures. A small tube containing a calibrated solution of indium-111 (400  $\mu$ L,  $\pm$  1.5 MBq) was positioned alongside the animal during scanning for the purpose of SPECT quantification. First, a scout view was performed using the X-CUBE (Molecubes, Ghent, Belgium) in a head-first prone position to establish the correct field of view (FOV). Subsequently, a CT scan was conducted with the previously determined FOV, employing a single projection with a 1 s exposure and X-rays at 55 kVp, with a total acquisition time of 5 min. After completing the CT scan, the scanning bed was transferred to a  $\gamma$ -CUBE (Molecubes) for static SPECT imaging (30 min), with energy peaks set at 171 and 246 keV and a window of  $\pm$ 10%. *In vivo*  $\mu$ SPECT/CT imaging was carried out at 1 and 24 h p.i. The

acquired SPECT images were reconstructed through a maximum-likelihood expectation-maximization (MLEM) algorithm using 10 iterations (Molecubes). The  $q$ -factor was determined from a volume of interest (VOI) that was drawn around the calibration tube and represents the ratio of counts/cc to activity/cc. This  $q$ -factor was subsequently incorporated during the preprocessing of the SPECT image prior to generating SUV-scaled images. SPECT/CT fusion and analysis were performed using PFUS version 4.0 (PMOD Technologies, Zurich, Switzerland).

**2.8. Statistical Analysis.** Statistical analysis was performed using Graph Pad Prism (version 9.5). The following tests were used, as described in each figure legend: ordinary one-way ANOVA with Tukey's multiple comparisons test, ordinary one-way ANOVA with Sidak's multiple comparisons test, two-way ANOVA with Tukey's multiple comparisons test, and unpaired  $t$  test. The differences were considered statistically significant for  $p < 0.05$ .

### 3. RESULTS AND DISCUSSION

**3.1. Synthesis of TPP-Containing Chelators.** We have used the compound 3-(aminopropyl)triphenylphosphonium (2) to functionalize the DOTA-based chelators with the delocalized lipophilic cation triphenyl phosphonium for mitochondria targeting, in the same way as we have previously reported for the synthesis of TPP-containing acyclic pyrazolyl diamine ligands.<sup>24</sup> As shown in Figure 2a, the synthesis of the single-targeted chelator TPP-DOTAGA was successfully achieved by the amide condensation reaction between the free amine of this TPP derivative and the commercially available DOTA-GA(*t*Bu)<sub>4</sub> (1), followed by removal of the *t*Bu protecting group by acid hydrolysis. After purification by solid phase extraction using Sep-Pak C18 cartridges with ACN/TFA 0.1% (aq) as eluents, the TPP-DOTAGA compound was characterized by multinuclear NMR spectroscopy, analytical HPLC and ESI-MS. In particular, the <sup>31</sup>P NMR spectrum (Figure S1) of TPP-DOTAGA showed a single peak at 24.07 ppm, which is compatible with the presence of an intact nonoxidized TPP group.

For the synthesis of dual-targeted DOTA-based chelators we have started from a DOTA prochelator bearing orthogonal protecting groups for a selective introduction of the TPP pharmacophore and KuE PSMA binding motif at opposite pendant arms of the macrocycle. Thus, this DOTA prochelator (2-[4,10-bis(2-*tert*-butoxy-2-oxo-ethyl)-7-(2-ethoxy-2-oxo-ethyl)-1,4,7,10-tetrazacyclododec-1-yl]acetic acid (4)), synthesized as we have previously described,<sup>35</sup> was reacted with compound 2 to afford a TPP-containing macrocycle (5) having *t*-butyl and ethyl-protected carboxylic acid pendant arms. Thereafter, the ethyl protecting group of compound 5 was removed by a careful basic hydrolysis. We have observed that prolonged times of reaction and temperatures higher than 50 °C could promote the oxidation of the TPP group. Thus, the hydrolysis reaction was run at 50 °C and was followed by HPLC analysis of aliquots from the reaction mixture to confirm its completion. After completion of the hydrolysis reaction, compound 6 was recovered by solid phase extraction using Sep-Pak C18 cartridges with 0.1% (aq) ACN/TFA as eluents and its chemical identity and purity confirmed by multinuclear NMR, analytical HPLC and ESI-MS (Figures S2–S4).

Initially, we have attempted the synthesis of TPP-DOTAGA-PSMA based on a solid-phase approach by reacting compound 6 with a Boc-protected PSMA-617 precursor supported in a Wang

resin obtained commercially from Pepmic, using procedures similar to those reported by other authors for the synthesis of PSMA-617 and related compounds.<sup>27,39</sup> However, in our hands, this solid-phase coupling reaction did not work in all the tested conditions (e.g., reagent concentrations, reaction time, or temperature). After reacting the resin with compound 6, its treatment with an appropriate cleavage cocktail always afforded the intact PSMA-617 precursor (data not shown). The reasons for this behavior were not clear but might reflect nonspecific hydrophobic binding of the TPP group to the resin surface. Thus, we have proceeded with the synthesis of TPP-DOTAGA-PSMA and congener TPP-DOTAGA-G<sub>3</sub>-PSMA using solution chemistry methodologies based on the reaction of compound 6 with the adequate *t*Bu protected PSMA derivatives (Figure 2c, i.e., compounds 9 and 11) that were synthesized as described in the Figure S5. In this case, the desired dual-targeted chelators were successfully synthesized and recovered in reasonably high yields after removal of the *t*OBu protecting groups by acidic hydrolysis with an appropriate cleavage cocktail and HPLC purification. TPP-DOTAGA-PSMA and TPP-DOTAGA-G<sub>3</sub>-PSMA were characterized by analytical HPLC and by ESI-MS that confirmed their chemical identity (Figures S6–S9).

**3.2. Synthesis, Characterization, and *In Vitro* Stability of <sup>111</sup>In complexes.** The <sup>111</sup>In-radiocomplexes with the different DOTA-based chelators under study, as well as their congeners with <sup>nat</sup>In, were obtained using the same synthetic approach that involved the complexation of the In<sup>3+</sup> ion in an aqueous acetate buffer solution (0.1 M, pH 5) upon heating at 95 °C for 30 min (Figure 3a). The complexes with <sup>nat</sup>In were obtained in almost quantitative yield by a complexation reaction performed at a 5:1 <sup>nat</sup>In/ligand molar ratio and purified by solid phase extraction (SPE) chromatography to discard the excess of In<sup>3+</sup>. The <sup>111</sup>In counterparts were also synthesized in high RCY (>95%) and with high molar activity by radiolabeling of the respective chelators used at a final 10 μM concentration. The <sup>111</sup>In complexes were submitted to purification by solid phase extraction (SPE) chromatography to eliminate any residual contaminants, like free In<sup>3+</sup> or insoluble indium hydroxides. After purification, all the radiocomplexes were obtained with an excellent radiochemical purity (>98%), as checked by radioHPLC analysis.

The complexes with <sup>nat</sup>In were characterized by analytical HPLC and ESI-MS (Figures S10–S16) and used as surrogates to identify the corresponding <sup>111</sup>In radiocomplexes by comparison of their HPLC retention times, as exemplified for <sup>nat</sup>In-TPP-DOTAGA-G<sub>3</sub>-PSMA in Figure 3b. The <sup>nat</sup>In-complexes were also used to determine the affinity for the PSMA receptor by competitive binding assays, as described below. The *in vitro* characterization of the <sup>111</sup>In-complexes involved also the study of their lipophilicity and radiochemical stability under physiological conditions, in cell culture medium, and in human serum.

The hydro/lipophilicity and/or the presence of different linkers between the KuE binding motif and the chelator framework can strongly influence the *in vitro* pharmacological properties, biodistribution, and pharmacokinetics of radiolabeled PSMA derivatives, as previously reported in several instances.<sup>30,40</sup> Thus, we have assessed the lipophilicity of the different <sup>111</sup>In complexes, based on the determination of their partition coefficients in *n*-octanol/0.1 M PBS pH 7.4 (Log  $D_{pH7.4}$ ), using the shake-flask method. The following Log  $D_{pH7.4}$  values were determined: [<sup>111</sup>In]In-TPP-DOTAGA:  $-3.42 \pm 0.04$ ; [<sup>111</sup>In]In-TPP-DOTAGA-PSMA:  $-2.67 \pm 0.05$ ;

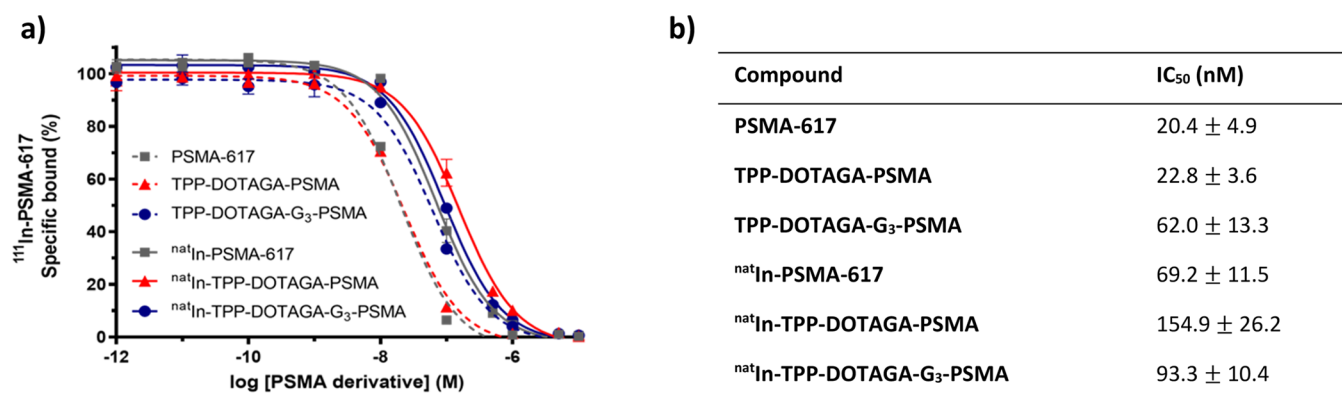


**Figure 4.** Competitive binding curves (a) and IC<sub>50</sub> values (b) determined for the nonradioactive PSMA derivatives under study. The binding curves were obtained by *in vitro* inhibition of [<sup>111</sup>In]In-PSMA-617 binding to PSMA on PC3 PIP cells using an increasing concentration of the tested compounds. Results are expressed as percentage of binding and were calculated from independent replicates (mean ± SEM, *n* = 3). The statistical difference between the IC<sub>50</sub> values was assessed by ordinary one-way ANOVA with Tukey's multiple comparisons test. All of the differences are statistically significant (*p* < 0.0001) with the exception of PSMA-617 vs TPP-DOTAGA-PSMA and TPP-DOTAGA-G<sub>3</sub>-PSMA vs <sup>nat</sup>In-PSMA-617.

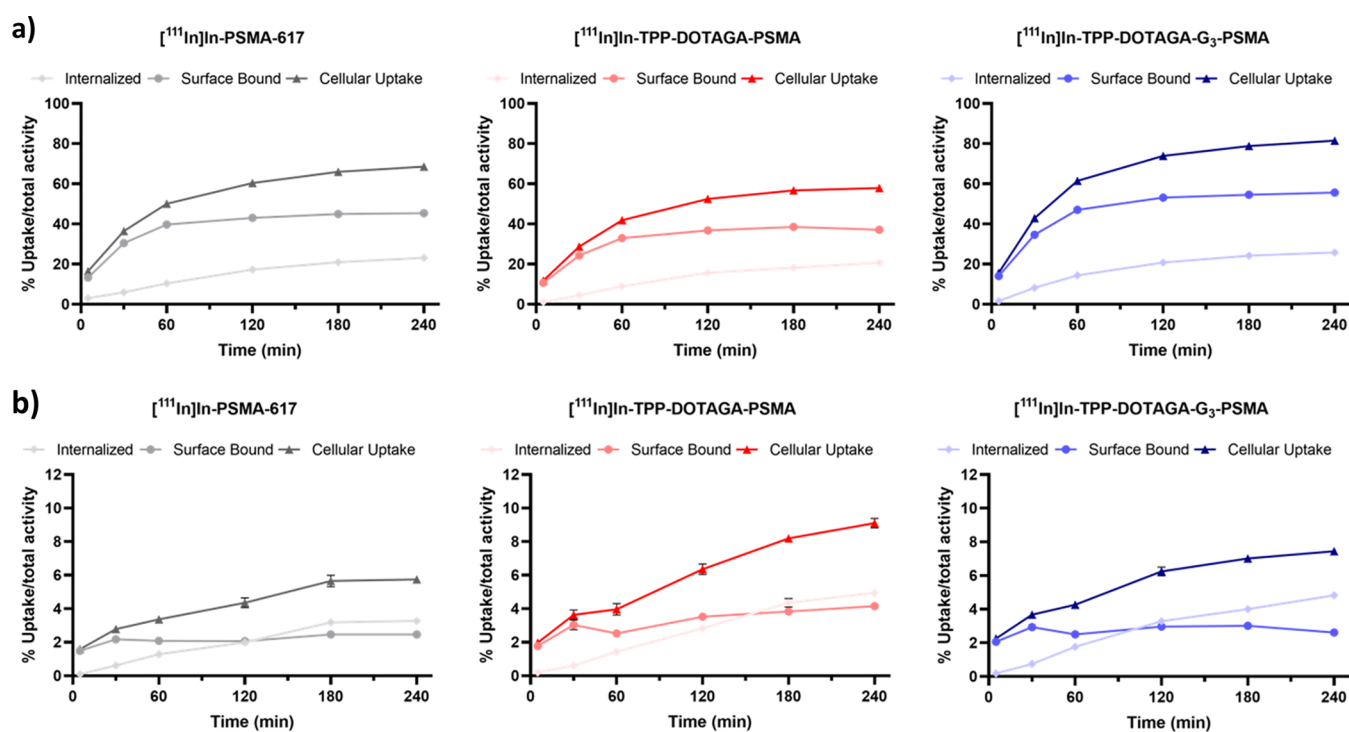


**Figure 5.** Time-dependent cellular uptake, surface-bound and internalization of the PSMA-targeted radiocomplexes a) PC3 PIP and b) LNCaP tumoral cells, at 37 °C. Results were expressed as a percentage of the total (applied) activity and were calculated from independent biological replicates (mean ± SEM; *n* = 4). The statistical difference between the internalization, surface bound and cellular uptake obtained for the different compounds at 240 min was assessed by ordinary one-way ANOVA with Tukey's multiple comparisons test. For PC3 PIP, all of the differences are statistically significant (*p* < 0.0001). For LNCaP, all of the differences are statistically significant (*p* < 0.0015) with the exception of the internalization of [<sup>111</sup>In]-In-TPP-DOTAGA-PSMA and [<sup>111</sup>In]-In-TPP-DOTAGA-G<sub>3</sub>-PSMA.

[<sup>111</sup>In]In-TPP-DOTAGA-G<sub>3</sub>-PSMA:  $-3.35 \pm 0.02$ ; [<sup>111</sup>In]In-PSMA-617:  $-3.56 \pm 0.03$ . All the complexes are hydrophilic with Log  $D_{pH7.4}$  values ranging between  $-2.67 \pm 0.05$  and  $-3.56 \pm 0.03$ , with the reference compound [<sup>111</sup>In]In-PSMA-617 being the most hydrophilic one. The Log  $D_{pH7.4}$  value of  $-3.56 \pm 0.03$  measured for [<sup>111</sup>In]In-PSMA-617 is less negative than the value of  $-4.1$  reported by other authors for this radiocomplex.<sup>41</sup> This difference certainly reflects the extremely high hydrophilicity of [<sup>111</sup>In]In-PSMA-617 that might hamper a very accurate determination of Log  $D_{pH7.4}$ . [<sup>111</sup>In]In-TPP-DOTAGA-PSMA is the least hydrophilic of the studied complexes with

a Log  $D_{pH7.4}$  value of  $-2.67 \pm 0.05$ , which reflects the introduction of the delocalized lipophilic cation TPP in one of the DOTA pendant arms. This effect is less pronounced for [<sup>111</sup>In]In-TPP-DOTAGA-G<sub>3</sub>-PSMA (Log  $D_{pH7.4}$  =  $-3.35 \pm 0.02$ ) certainly due to the presence of the hydrophilic Gly-Gly-Gly linker between the KuE binding motif and the DOTA framework.

The stability of the <sup>111</sup>In-radiocomplexes was evaluated upon incubation of the complexes with phosphate-buffered saline (PBS) pH 7.4, in cell culture medium (RPMI) and in human serum at 37 °C. Analysis of the samples by RP-HPLC showed

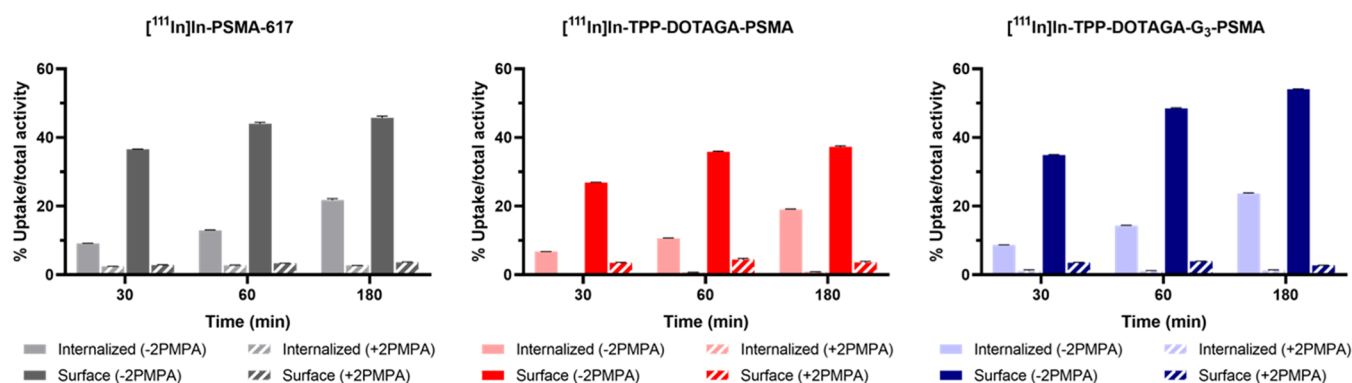


**Figure 6.** PSMA-blocking study with 2-PMPA (100  $\mu$ M/0.5 mL/well) in PC3 PIP cells at 37  $^{\circ}$ C: Cell surface-bound and internalization of [<sup>111</sup>In]In-TPP-DOTAGA-PSMA, [<sup>111</sup>In]In-TPP-DOTAGA-G<sub>3</sub>-PSMA, and [<sup>111</sup>In]In-PSMA-617 incubated with or without 2-PMPA for 30, 60, and 180 min. Data was expressed as a percentage of the total (applied) activity. Results were calculated from independent biological replicates ( $n = 4$ ), and are given as the mean  $\pm$  SEM. For each compound at each time point, the statistical difference between the values of internalization or surface bound with or without addition of 2-PMPA was assessed by ordinary one-way ANOVA with Sidak's multiple comparisons test. All of the differences are statistically significant ( $p < 0.0001$ ).

that all the complexes are stable up to 48 h (Figures S17–S20), in all tested conditions and as exemplified for [<sup>111</sup>In]In-TPP-DOTAGA-G<sub>3</sub>-PSMA in Figure 3c. This result showed that all of the radiocomplexes retained their chemical integrity in the cellular assays described below, even at the longest tested incubation time of 48 h.

**3.3. In Vitro PSMA-Binding Affinity.** The receptor-binding affinities of PSMA-bearing chelators and In-complexes for the human PSMA receptor were determined by competition-binding assays against HPLC-purified [<sup>111</sup>In]In-PSMA-617, as recently described by other authors.<sup>41</sup> The study was performed in PC3 PIP cells, and all PSMA derivatives displaced the radioligand from the PSMA-binding sites in a concentration-dependent way. The best-fit IC<sub>50</sub> values (Figure 4b) were determined from the competitive receptor-binding curves, represented in Figure 4a, by fitting the data with a nonlinear regression.

The IC<sub>50</sub> value determined for dual-targeted chelator TPP-DOTAGA-PSMA (22.8  $\pm$  3.6 nM) is similar to the one obtained for PSMA reference chelator PSMA-617 (20.4  $\pm$  4.9 nM), while TPP-DOTAGA-G<sub>3</sub>-PSMA (62.0  $\pm$  13.3 nM) showed a statistically significant higher value. These values are in the same order of magnitude of the IC<sub>50</sub> values reported in the literature for high-affinity PSMA ligands,<sup>30,40,42</sup> despite different radioligands and/or cell lines were used to perform the competitive binding assays. In particular, the IC<sub>50</sub> of 20.4 nM obtained for PSMA-617 is relatively similar to the 9 nM value reported recently for this compound, when the competitive binding assay was performed in LS174T-PSMA cells using [<sup>111</sup>In]In-PSMA-617 as the radioligand.<sup>41</sup>

The complexation with In<sup>3+</sup> resulted in a slightly lower binding affinity for the resulting complexes when compared with those of the respective free chelators. The IC<sub>50</sub> value of <sup>nat</sup>In-TPP-DOTAGA-G<sub>3</sub>-PSMA (93.3  $\pm$  10.4 nM) is more comparable to that of <sup>nat</sup>In-PSMA-617 (69.2  $\pm$  11.5 nM) contrary to the IC<sub>50</sub> calculated for the <sup>nat</sup>In-TPP-DOTAGA-PSMA complex (154.9  $\pm$  26.2 nM), reversing the trend observed for the respective free chelators. All in all, the competitive binding assays showed that introduction of the TPP moiety and Gly-Gly-Gly linker did not compromise the ability of the dual-targeted complexes to recognize the PSMA protein.

**3.4. Cellular Uptake, Internalization, and Blockade Assays.** The ability of the dual-targeting complexes ([<sup>111</sup>In]In-

TPP-DOTAGA-PSMA and [<sup>111</sup>In]In-TPP-DOTAGA-G<sub>3</sub>-PSMA) and related single-targeting complexes ([<sup>111</sup>In]In-TPP-DOTAGA and [<sup>111</sup>In]In-PSMA-617) to be taken up and internalized by PSMA+ tumor cells was assessed in PC3 PIP and LNCaP cells. The human prostate cancer cell line LNCaP was used for comparison, as this cell line endogenously expresses PSMA, although in moderate levels (Figure S21). As a control, the same cellular assays were run in PSMA-negative PC3 (PC3 flu) human prostate cancer cells. It is important to notice that all the cellular assays were performed using radiocomplexes obtained with the same molar activities (typically 15 MBq/nmol). It is well-known that the molar activity of PSMA-targeted radioconjugates might have a dramatic influence on their ability to bind PSMA, both in cellular or animal models, due to different degrees of receptor blockade by the cold ligands.<sup>43,44</sup>

The cellular uptake, surface-bound fraction, and internalization of the radiocomplexes in the different cell lines were studied by incubation with the desired compound at 37  $^{\circ}$ C, for up to 4 h. The results are presented in Figure 5 and in Figure S22.

As shown in Figure 5a, the different PSMA-targeted <sup>111</sup>In-complexes have similar kinetics of uptake and internalization in the PC3 PIP cells. After 4 h of incubation, the values almost reached a plateau which varied between 57.9 and 81.5% for the cellular uptake and between 20.7 and 25.8% for the internalization fraction, following the order [<sup>111</sup>In]In-TPP-DOTAGA-PSMA < [<sup>111</sup>In]In-PSMA-617 < [<sup>111</sup>In]In-TPP-DOTAGA-G<sub>3</sub>-PSMA. The lowest uptake and internalization rates found for [<sup>111</sup>In]In-TPP-DOTAGA-PSMA probably reflects its lowest binding affinity toward the PSMA receptor, which was assessed in the PC3 PIP cells by competitive binding assays (see Figure 4). Nevertheless, the cellular uptake and internalization processes are not influenced only by the binding affinity of the radioconjugates toward the PSMA, depending also on their intracellular localization and residualization that determine their efflux rate from the cells. In fact, [<sup>111</sup>In]In-TPP-DOTAGA-G<sub>3</sub>-PSMA showed a slightly lower PSMA affinity than [<sup>111</sup>In]In-PSMA-617 but presented the highest uptake and internalization in the PC3 PIP cells.

For all the PSMA-targeted <sup>111</sup>In-complexes, their uptake and internalization in LNCaP cells (Figure 5b) were 5- to 10-fold lower than in PC3 PIP cells, due most probably to the higher PSMA expression level in the latter cell line (Figure S21). The dual-targeted complexes [<sup>111</sup>In]In-TPP-DOTAGA-PSMA and

$[^{111}\text{In}]\text{In-TPP-DOTAGA-G}_3\text{-PSMA}$  showed minimal binding and internalization in the PSMA negative PC3 flu cells (Figure S22) with internalized fractions after 4 h of incubation of only 0.13% and 0.14%, respectively. The compound  $[^{111}\text{In}]\text{In-PSMA-617}$  presented higher uptake (3.5–3.8%) and internalization values (2.1–2.2%) in this PSMA negative cell line, which however were constant over time. These results show that the introduction of the lipophilic TPP pharmacophore did not promote nonspecific binding or uptake in PCa cells. Consistently, we have verified that  $[^{111}\text{In}]\text{In-TPP-DOTAGA}$ , without the PSMA targeting vector, has a negligible cell uptake in the different tested cell lines (PC3 PIP, PC3 flu and LNCaP) (Figure S23).

The involvement of PSMA-mediated processes in the cell binding of  $[^{111}\text{In}]\text{In-TPP-DOTAGA-PSMA}$ ,  $[^{111}\text{In}]\text{In-TPP-DOTAGA-G}_3\text{-PSMA}$ , and  $[^{111}\text{In}]\text{In-PSMA-617}$  was first indicated by their much higher uptake and internalization in the PSMA+ PC3 PIP cells than in the PSMA- PC3 flu tumoral cells. To further demonstrate a PSMA-specific uptake, we performed blockade assays in PC3 PIP cells using the well-known PSMA inhibitor 2-PMPA.

As shown in Figure 6, the PSMA blocking with excess 2-PMPA (100  $\mu\text{M}$ ) almost completely prevented the binding and internalization of  $[^{111}\text{In}]\text{In-TPP-DOTAGA-PSMA}$  and  $[^{111}\text{In}]\text{In-TPP-DOTAGA-G}_3\text{-PSMA}$  in PC3 (92–95% and 87–95% inhibition for 30–180 min incubation, respectively (see Figure S24), even in a higher extent compared with the reference compound  $[^{111}\text{In}]\text{In-PSMA-617}$  (73–88% inhibition, Figure S24). These results confirm that the dual-targeted complexes are less prone to suffer nonspecific binding processes compared to the reference compound  $[^{111}\text{In}]\text{In-PSMA-617}$ , undergoing essentially a PSMA-specific cell uptake.

**3.5. Subcellular Localization: Nuclear and Mitochondrial Uptake.** Next, we have studied the subcellular localization of the PSMA-targeted radioconjugates in PC3 PIP cells to assess how the presence of the TPP affects their distribution, namely, the accumulation in the mitochondria that was thought as the subcellular radiosensitive target of the TPP-containing complexes. We have also studied the nuclear uptake of the different PSMA-targeted  $^{111}\text{In}$ -complexes, as nuclear DNA still is considered the “canonical” target of AE emitters to obtain enhanced radiotoxic effects.

The nuclear uptake was assessed after incubation with the  $^{111}\text{In}$ -labeled complexes and, as shown in Figure 7, the fraction of the compounds that entered the nucleus was relatively small (about 2–4% of the total cell uptake), with  $[^{111}\text{In}]\text{In-TPP-DOTAGA-PSMA}$  presenting the highest value at 120 min.

Then, the mitochondrial uptake of the different radio-complexes was evaluated using the Mitochondria Isolation Kit of Miltenyi Biotec. Mitochondria were magnetically labeled with Anti-TOM22 MicroBeads, where the monoclonal Anti-TOM22 antibody specifically binds to the translocase of outer mitochondrial membrane 22 (TOM22) of human mitochondria and then separated from the other organelles using a magnetic field. The results for mitochondrial uptake of the radio-complexes expressed as percentage of the cellular uptake and percentage of applied activity after 1 h of incubation are presented in Figure 8, and those for after 2 h of incubation are presented in Figure S25.

The dual-targeted complexes  $[^{111}\text{In}]\text{In-TPP-DOTAGA-PSMA}$  and  $[^{111}\text{In}]\text{In-TPP-DOTAGA-G}_3\text{-PSMA}$  were expected to show an increased mitochondrial uptake compared to the single-targeted congener  $[^{111}\text{In}]\text{In-PSMA-617}$  due to the

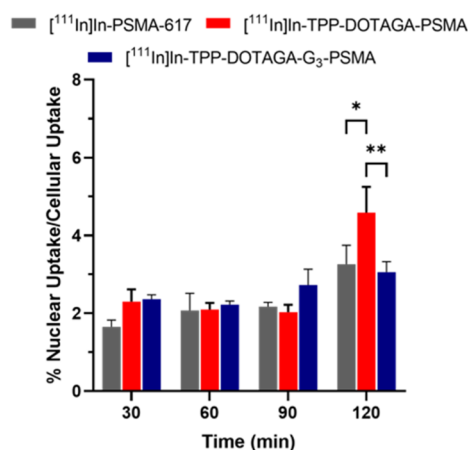


**Figure 7.** Nuclear uptake of  $[^{111}\text{In}]\text{In-PSMA-617}$ ,  $[^{111}\text{In}]\text{In-TPP-DOTAGA-PSMA}$ , and  $[^{111}\text{In}]\text{In-TPP-DOTAGA-G}_3\text{-PSMA}$  in PC3 PIP cells at 37 °C, after incubation from 30 to 120 min. Results were expressed as a percentage of the cell-associated activity and were calculated from independent biological replicates (mean  $\pm$  SEM;  $n = 3$ ). The statistical difference between the nuclear uptake of the different compounds at each time point was assessed by two-way ANOVA with Tukey’s multiple comparisons test (\*  $p < 0.05$ , \*\*  $p < 0.01$ ).

presence of the mitochondrion-tropic TPP pharmacophore. However, the mitochondrial uptake expressed as percentage of the cellular uptake is similar for all compounds at both studied time points (i.e., 1 and 2 h of incubation), ranging between 7.8 and 10.2%. However, for 1 h of incubation,  $[^{111}\text{In}]\text{In-TPP-DOTAGA-G}_3\text{-PSMA}$  presented the highest value of mitochondrial uptake, expressed as percentage of the applied activity (i.e., 2.8% compared to the 1.7 and 1.6% values found for  $[^{111}\text{In}]\text{In-TPP-DOTAGA-PSMA}$  and  $[^{111}\text{In}]\text{In-PSMA-617}$ , respectively (although not statistically significant)). Most probably, this trend reflects the highest internalization rate of  $[^{111}\text{In}]\text{In-TPP-DOTAGA-G}_3\text{-PSMA}$  eventually related with an augmented residualization of this complex due to the intracellular cleavage of the GlyGlyGly linker by cathepsin B. These results seem to indicate that the presence of the TPP pharmacophore does not confer pronounced mitochondria-tropic characteristics to the final radioconjugates, which might reflect their high hydrophilicity, overall negative charge, and molecular size.

**3.6. Survival Assays.** Clonogenic assays reflect the ability of cells to divide and to form colonies, being the most used assay to assess radiocytotoxic effects in cancer cells exposed to high linear energy transfer (LET) radiation, namely, Auger electrons.<sup>45</sup> Having this in mind, we have performed clonogenic assays in PC3 PIP and PC3 flu cells that were exposed, during 24 h at 37 °C, to increasing activities (0–1.85 MBq) of the PSMA-targeted complexes  $[^{111}\text{In}]\text{In-PSMA-617}$ ,  $[^{111}\text{In}]\text{In-TPP-DOTAGA-PSMA}$ , and  $[^{111}\text{In}]\text{In-TPP-DOTAGA-G}_3\text{-PSMA}$ . PC3 PIP cells suffered a reduction of their survival in a dose-dependent manner (Figure 9a), while there was no effect on PC3 flu cells (Figures S26) which is in line with the negligible internalization of the radiocomplexes in PC3 flu cells.

Figure 9a presents a comparison of the cell survival fractions of PC3 PIP cells exposed for 24 h to increasing activities of the different PSMA-targeted complexes. The highest effect was observed for  $[^{111}\text{In}]\text{In-TPP-DOTAGA-G}_3\text{-PSMA}$  with almost 60% reduction of cell survival, while  $[^{111}\text{In}]\text{In-TPP-DOTAGA-PSMA}$  had the least effect on cell survival. For example,  $[^{111}\text{In}]\text{In-TPP-DOTAGA-PSMA}$  exerted almost no effect on the cell survival for the 0.74 MBq activity, but at this activity

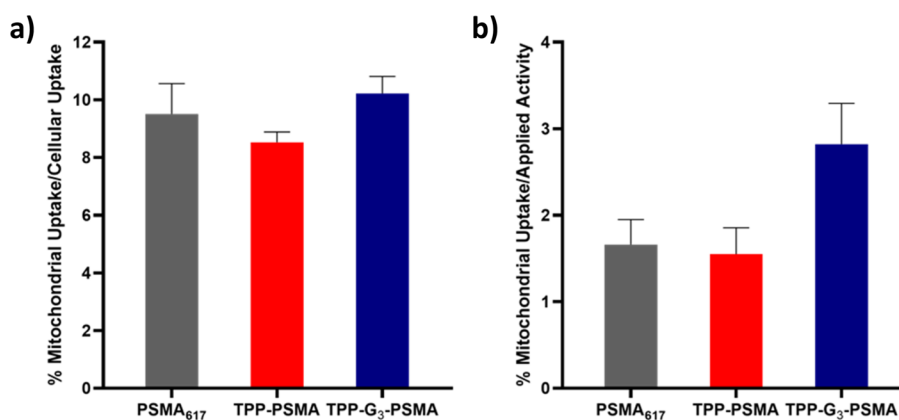


**Figure 8.** Mitochondrial uptake of [<sup>111</sup>In]In-PSMA-617, [<sup>111</sup>In]In-TPP-DOTAGA-PSMA, and [<sup>111</sup>In]In-TPP-DOTAGA-G<sub>3</sub>-PSMA in PC3 PIP cells at 37 °C after 1 h incubation expressed as a percentage of (a) cellular uptake and (b) applied activity. For the sake of simplicity, these radiocomplexes are noted in the graphs as PSMA<sub>617</sub>, TPP-PSMA, and TPP-G<sub>3</sub>-PSMA, respectively. Results were expressed as a percentage of the cell-associated activity and as a percentage of the applied activity and were calculated from independent biological replicates (mean ± SEM; *n* = 2). The statistical difference between the mitochondrial uptake of the different compounds was assessed by ordinary one-way ANOVA with Tukey's multiple comparisons test. The differences are not statistically significant.

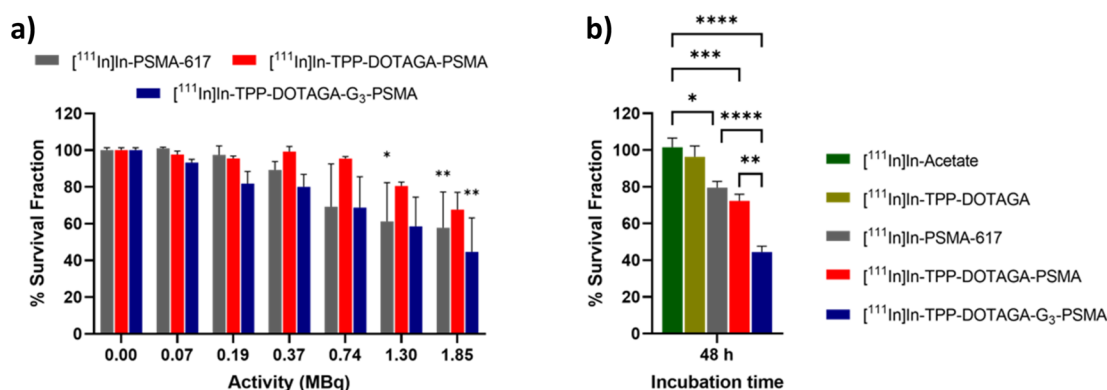


**Figure 9.** Results of the clonogenic assays in PC3 PIP cells: a) Survival fractions after 24 h incubation of the cells with 0–1.85 MBq of [<sup>111</sup>In]In-PSMA-617, [<sup>111</sup>In]In-TPP-DOTAGA-PSMA, and [<sup>111</sup>In]In-TPP-DOTAGA-G<sub>3</sub>-PSMA, at 37 °C. Data correspond to mean ± SEM (*n* = 3 replicates). The statistical difference between the survival fractions with respect to the control (0.00 MBq) was assessed by two-way ANOVA with Tukey's multiple comparisons test (\* *p* < 0.05, \*\* *p* < 0.01). b) Survival fraction after 48 h incubation of the cells with 0.74 MBq of [<sup>111</sup>In]In-PSMA-617, [<sup>111</sup>In]In-TPP-DOTAGA, [<sup>111</sup>In]In-TPP-DOTAGA-PSMA, [<sup>111</sup>In]In-TPP-DOTAGA-G<sub>3</sub>-PSMA, and [<sup>111</sup>In]In-acetate. Data correspond to mean ± SEM (*n* = 6 replicates). The statistical difference between the survival fractions of different compounds was assessed by ordinary one-way ANOVA with Tukey's multiple comparisons test (\* *p* < 0.05, \*\* *p* < 0.01, \*\*\* *p* < 0.001, \*\*\*\* *p* < 0.0001). Results for [<sup>111</sup>In]In-acetate (<sup>111</sup>In-Ac) and [<sup>111</sup>In]In-TPP-DOTAGA are not statistically different.

[<sup>111</sup>In]In-PSMA-617 and [<sup>111</sup>In]In-TPP-G<sub>3</sub>-PSMA reduced the cell survival fraction to ca. 69%. The later radiocomplexes showed very similar effects on the cell survival with the exception of the highest tested activity of 1.85 MBq, for which [<sup>111</sup>In]In-TPP-DOTAGA-G<sub>3</sub>-PSMA seemed more efficient to compromise the cell survival compared to [<sup>111</sup>In]In-PSMA-617 (although not statistically significant), leading the compounds to 45 and 58% cell survival fractions, respectively.

To have a clearer view on the efficiency of the different compounds to elicit radiocytotoxic effects and compromise cell survival, we performed clonogenic survival assays in PC3 PIP cells exposed for 48 h to 0.74 MBq of each compound. By considering a longer time of exposure, we expected that an increased number of accumulated decays would enhance the radiotoxic effects with better discrimination of the action of the different PSMA-targeted complexes. In addition to [<sup>111</sup>In]In-PSMA-617, [<sup>111</sup>In]In-TPP-DOTAGA-PSMA and [<sup>111</sup>In]In-TPP-DOTAGA-G<sub>3</sub>-PSMA, the study involved also the single-targeted [<sup>111</sup>In]In-TPP-DOTAGA and [<sup>111</sup>In]In-acetate as controls, and the results are presented in Figure 9b. [<sup>111</sup>In]In-

TPP-DOTAGA and [<sup>111</sup>In]In-acetate led to the highest survival fractions with a negligible inhibition of cellular proliferation that certainly results from their inability to bind to the PSMA+ PC3 cells. Considering the PSMA-targeted radiocomplexes, [<sup>111</sup>In]In-TPP-DOTAGA-G<sub>3</sub>-PSMA was the most efficient compound inducing a remarkably higher reduction (about 55%) of the survival of PC3 PIP cells when compared with the single-targeted congener [<sup>111</sup>In]In-PSMA-617 that induced a 20–28% reduction of the cell survival.

The highest ability of [<sup>111</sup>In]In-TPP-DOTAGA-G<sub>3</sub>-PSMA to compromise the survival of PC3 PIP cells is probably related with its highest cellular uptake and internalization compared with the other PSMA-targeted <sup>111</sup>In-complexes and not necessarily due to different subcellular distribution and localization. In fact, the subcellular localization studies have shown that all the complexes have relatively similar mitochondrial uptakes, when expressed as percentage of the activity associated with the cells. Thus, apparently, the potentially different mitochondria tropic properties of the complexes do not play an important role to discriminate the induced radio-

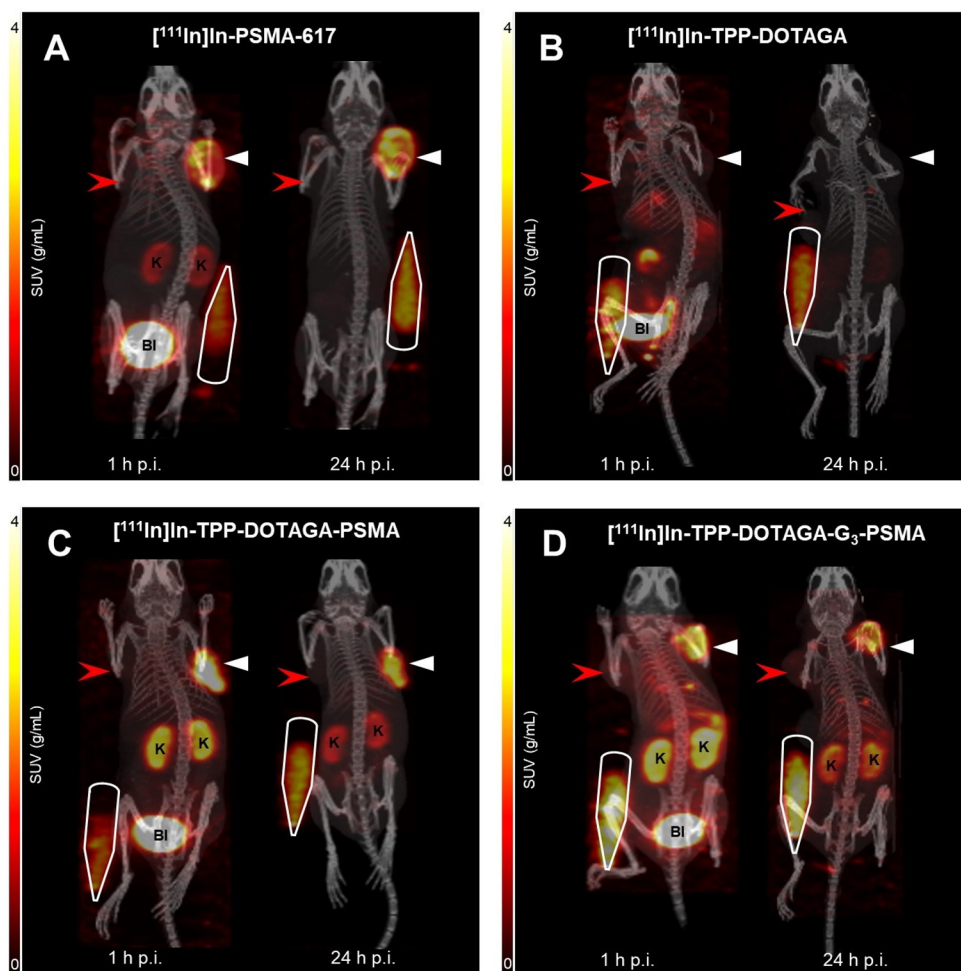


**Figure 10.** Fused SPECT-CT images with maximum intensity projections (MIP) of SPECT at 1 and 24 h p.i. of one representative mouse from each experimental group: [ $^{111}\text{In}$ ]In-PSMA-617 (A), [ $^{111}\text{In}$ ]In-TPP-DOTAGA (B), [ $^{111}\text{In}$ ]In-TPP-DOTAGA-PSMA (C), and [ $^{111}\text{In}$ ]In-TPP-DOTAGA- $\text{G}_3$ -PSMA (D). PSMA-positive tumors are indicated by a white triangle, whereas PSMA-negative tumors are represented by a red arrowhead. Calibration tubes are outlined with a solid white line. Kidneys are marked as “K” and bladder as “Bl”.

biological effects. Nevertheless, [ $^{111}\text{In}$ ]In-TPP-DOTAGA- $\text{G}_3$ -PSMA showed the highest absolute mitochondrial uptake for the shortest incubation time of 1 h, certainly due to its highest internalization rate.

We should mention that it has been described that PSMA inhibitors overtime present a homogeneous distribution in the cytoplasm of prostate cancer cells, after internalization and dissociation of the PSMA/PSMA inhibitor complexes during the PSMA recycling process in the endosomes.<sup>46</sup> This homogeneous distribution naturally also includes the cytoplasmic perinuclear region, and this localization in nuclear proximity can enhance local radiation doses by radiolabeled PSMA inhibitors and induce pronounced cell death, in particular, for high LET particles like Auger electrons. Such reasoning has been invoked by Pomper et al. to explain the antitumoral efficacy of the  $^{125}\text{I}$ -labeled PSMA inhibitor 2-[3-[1-carboxy-5-(4-[ $^{125}\text{I}$ ]iodo-benzoylamino)-pentyl]-ureido]-pentanedioic acid ( $^{125}\text{I}$ -DCIBzL) both in tumor cellular models and in PCa xenografts.<sup>47,48</sup> Eventually, the highest *in vitro* antitumor efficacy found for [ $^{111}\text{In}$ ]In-TPP-DOTAGA- $\text{G}_3$ -PSMA can be explained by its highest internalization in PC3 PIP cells that leads to an augmented number of decays in the cytoplasmic perinuclear region, therefore increasing the probability of direct nuclear DNA hits by the emitted AEs. For the same reason, one

cannot also exclude a greater contribution of mitochondrial irradiation in the case of [ $^{111}\text{In}$ ]In-TPP-DOTAGA- $\text{G}_3$ -PSMA when compared with those of [ $^{111}\text{In}$ ]In-TPP-DOTAGA-PSMA and [ $^{111}\text{In}$ ]In-PSMA-617.

**3.7.  $\mu\text{SPECT}$  Imaging Studies in PCa xenografts.** In addition to the *in vitro* evaluation of dual targeting efficacy using TPP and a PSMA-binding motif, an *in vivo* PCa mouse model was generated. Specifically, a PSMA-negative (PC3-Flu) and a PSMA-positive cell line (PC3-PIP) were implanted on the left and right flanks of a SCID/Beige mouse, respectively. In order to assess the dual-targeting efficacy, two tracers were injected: [ $^{111}\text{In}$ ]In-TPP-DOTAGA-PSMA and [ $^{111}\text{In}$ ]In-TPP-DOTAGA- $\text{G}_3$ -PSMA. To compare the pharmacokinetic profile to single-targeting tracers, two additional control groups were introduced: [ $^{111}\text{In}$ ]In-PSMA-617 and [ $^{111}\text{In}$ ]In-TPP-DOTAGA. The maximum intensity projection (MIP) images and the  $\mu\text{SPECT}$ -based SUV data obtained for each radiocomplex are presented in Figures 10 and 11, respectively.

In the single-targeting reference group, [ $^{111}\text{In}$ ]In-PSMA-617 showed fast renal clearance with substantial uptake at 1 h p.i. observed in PSMA-positive tumors (SUV 1.39), while minimal tracer accumulation was observed in PSMA-negative tumors (SUV 0.14). Additionally, there was low tracer uptake in the kidneys (SUV 0.65) at this time point. At 24 h p.i., most of the

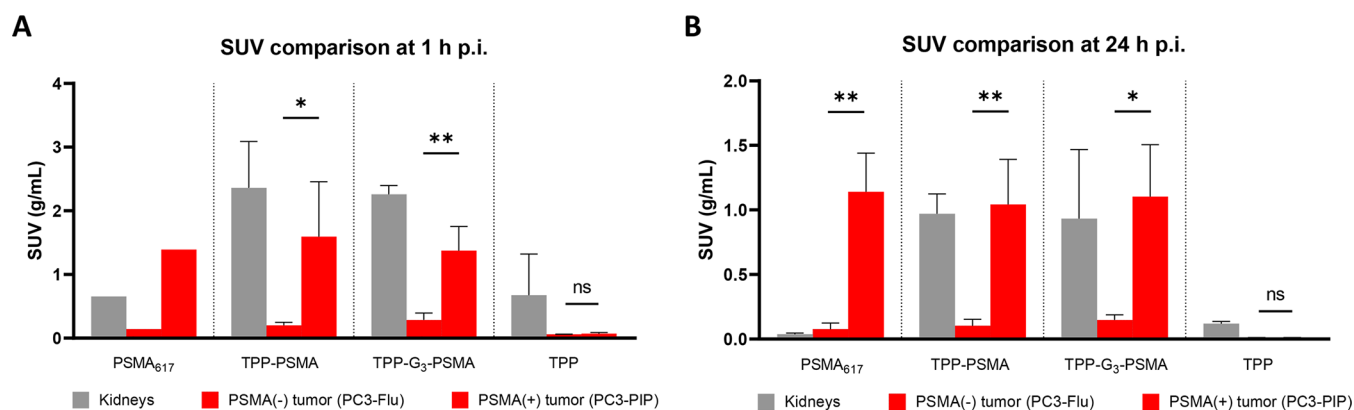


**Figure 11.** Comparison of  $\mu$ SPECT-based SUV data of [ $^{111}\text{In}$ ]In-PSMA-617, [ $^{111}\text{In}$ ]In-TPP-DOTAGA-PSMA, [ $^{111}\text{In}$ ]In-TPP-DOTAGA-G<sub>3</sub>-PSMA, and [ $^{111}\text{In}$ ]In-TPP-DOTAGA at 1 h (A) and 24 h (B) p.i. For the sake of simplicity, these radiocomplexes are noted in the graphs as PSMA<sub>617</sub>, TPP-PSMA, TPP-G<sub>3</sub>-PSMA, and TPP, respectively. Error bars represent the standard error of the means (SEM) with  $n = 3$  for all groups except for [ $^{111}\text{In}$ ]In-PSMA-617 at 1 h ( $n = 2$ ). The statistical difference between PSMA-negative and positive tumor uptake was assessed using an unpaired  $t$  test (\*  $p < 0.05$ , \*\*  $p < 0.01$ ).

activity had cleared from both the kidneys and PSMA-negative tumors, but the tracer showed retention in PSMA-positive tumors. As expected, [ $^{111}\text{In}$ ]In-TPP-DOTAGA did not show a significant uptake in PSMA-expressing tumors.

Upon addition of a mitochondria-targeting pharmacophore, TPP, the dual-targeting tracer [ $^{111}\text{In}$ ]In-TPP-DOTAGA-PSMA demonstrated fast renal clearance and comparable PSMA specific tumor uptake at 1 and 24 h p.i. as the reference tracer [ $^{111}\text{In}$ ]In-PSMA-617. Similarly, there was minimal uptake in PSMA-negative tumors (SUV 0.20) but considerable uptake in PSMA-expressing tumors (SUV 1.59). Notably, the inclusion of TPP resulted in a substantial increase in kidney uptake at 1 h p.i. (SUV 2.36), which decreased to SUV 1.04 at 24 h. The same profile was observed in the second dual-targeting tracer that is equipped with a cleavable triglycine linker between TPP-DOTAGA and the PSMA-binding motif ([ $^{111}\text{In}$ ]In-TPP-DOTAGA-G<sub>3</sub>-PSMA). As such, the introduction of TPP with or without cleavable linker (G<sub>3</sub>) did not affect the pharmacokinetics and tumor uptake in PSMA-positive or -negative xenograft sites. However, there is substantial evidence that introducing TPP to PSMA-based tracers considerably increases kidney uptake and retention.

The increased kidney uptake observed for the dual tracers cannot be attributed directly to the TPP moiety since complex [ $^{111}\text{In}$ ]In-TPP-DOTAGA did not show significant uptake in the kidney. Nonetheless, the introduction of the positively charged TPP moiety in the PSMA-targeted tracer modifies the overall charge and lipophilicity of the dual targeted complexes, which can eventually justify the increased kidney uptake.<sup>40</sup> The increased renal uptake is a concern, especially for radiopharmaceuticals to be used in therapy. However, we would like to emphasize that kidney damage due to radiotoxic effects is not well studied for Auger/conversion electrons emitters like  $^{111}\text{In}$ , when compared to  $\beta^-$  emitters like  $^{90}\text{Y}$  or  $^{177}\text{Lu}$ . Most likely, the short tissue range of AEs should avoid a significant renal injury in comparison to treatment with the long-ranged  $\beta^-$  particles, even for a high renal uptake. For example, Müller and collaborators have shown that Auger/conversion electrons do not increase overall renal damage as evidenced by comparing the effects induced by  $^{161}\text{Tb}$ -folate and  $^{177}\text{Lu}$ -folate.<sup>49</sup> In addition,  $^{111}\text{In}$ -octreotide used as an AE-emitting radiotherapeutic in a clinical trial did not impair kidney function up to a renal dose of 45 Gy. This result was explained by the fact that Auger/conversion

electrons are unable to damage the radiosensitive glomeruli and potential cell damage is limited to the more radioresistant tubular cells, accumulating the radioconjugates.<sup>8</sup>

#### 4. CONCLUSIONS

We have succeeded in the synthesis of novel dual-targeting compounds ([ $^{111}\text{In}$ ]In-TPP-DOTAGA-PSMA and [ $^{111}\text{In}$ ]In-TPP-DOTAGA-G<sub>3</sub>-PSMA) that were obtained with high RCY and high molar activities. The *in vitro* studies demonstrated that these compounds maintained their integrity under physiological conditions and in cell culture media and showed relatively similar binding affinities toward PSMA, compared to the reference tracer [ $^{111}\text{In}$ ]In-PSMA-617 and using competitive binding assays. Nevertheless, the metal complexation and the presence of the Gly-Gly-Gly linker showed some influence on the binding affinity of the compounds. To better understand these effects, *in silico* approaches based on molecular docking and molecular dynamics simulations are a good option, as previously reported by other authors for different families of PSMA inhibitors,<sup>39,50,51</sup> taking advantage of the availability of the X-ray structure of the PSMA protein.<sup>52</sup> However, these *in silico* studies were outside the scope of the present work.

Cellular uptake and internalization experiments in PSMA-positive cells (PC3 PIP) revealed efficient internalization of all PSMA-targeted complexes, while PSMA-negative cells (PC3 Flu) showed negligible uptake. [ $^{111}\text{In}$ ]In-TPP-DOTAGA-G<sub>3</sub>-PSMA had the highest internalization rate in PC3 PIP cells and the highest initial mitochondrial uptake, which certainly justify the enhanced radiocytotoxic effects exhibited by this compound in the same cell line. However, apparently, the tested TPP-containing radioconjugates do not show a pronounced mitochondria-tropic nature, due most probably to their high hydrophilicity, overall negative charge, and molecular size. Taking advantage of the versatility of our bifunctional chelators, we expect to fine-tune these properties by using different linkers to attach the TPP or PSMA-617 moieties to the chelator framework.

*In vivo*  $\mu$ SPECT data indicated a comparable pharmacokinetic profile for the PSMA targeting constructs [ $^{111}\text{In}$ ]In-TPP-DOTAGA-PSMA and [ $^{111}\text{In}$ ]In-TPP-DOTAGA-G<sub>3</sub>-PSMA in terms of blood and tissue clearance and specific PSMA tumor uptake, but revealed increased renal uptake compared to that of the control construct [ $^{111}\text{In}$ ]In-PSMA-617. High kidney

uptake is an unfavorable issue that is often found in the development of PSMA-targeted radiopharmaceuticals. Fortunately, previous therapeutic studies in animal models and patients indicate that the Auger electrons and low energy conversion electrons do not result in additional renal injury.<sup>8,49</sup> Moreover, several strategies can be used to circumvent this issue which includes the coadministration of blocking agents (e.g., PMPA or monosodium glutamate)<sup>53,54</sup> or reduction of the effective molar activity of the administered radiopharmaceutical.<sup>44</sup>

In conclusion, our results provide valuable insights into the design and potential use of mitochondrial targeting of PSMA-based radiocomplexes for efficient use of AE-emitting radionuclides in targeted radionuclide therapy, giving impetus to extend the studies to other AE-emitting trivalent radiometals (e.g., <sup>161</sup>Tb or <sup>165</sup>Er) and to further optimize the designed dual-targeting constructs.

## ■ ASSOCIATED CONTENT

### SI Supporting Information

The Supporting Information is available free of charge at <https://pubs.acs.org/doi/10.1021/acs.molpharmaceut.3c00787>.

Description of the chemical synthesis of PSMA precursors; additional figures for the (i) synthesis and characterization of TPP-containing chelators, (ii) synthesis, characterization and *in vitro* stability of In-complexes, (iii) cellular uptake, internalization and blockade assays, (iv) clonogenic survival assays (PDF)

## ■ AUTHOR INFORMATION

### Corresponding Author

**António Paulo** – *C<sup>2</sup>TN – Centro de Ciências e Tecnologias Nucleares Instituto Superior Técnico, Universidade de Lisboa, 2695-066 Bobadela LRS, Portugal; DECN – Departamento de Engenharia e Ciências Nucleares, Instituto Superior Técnico, Universidade de Lisboa, 2695-066 Bobadela LRS, Portugal; [orcid.org/0000-0002-9164-0913](https://orcid.org/0000-0002-9164-0913); Email: [apaulo@tecnico.ulisboa.pt](mailto:apaulo@tecnico.ulisboa.pt)*

### Authors

**Joana F. Santos** – *C<sup>2</sup>TN – Centro de Ciências e Tecnologias Nucleares Instituto Superior Técnico, Universidade de Lisboa, 2695-066 Bobadela LRS, Portugal*

**Maria T. Braz** – *C<sup>2</sup>TN – Centro de Ciências e Tecnologias Nucleares Instituto Superior Técnico, Universidade de Lisboa, 2695-066 Bobadela LRS, Portugal*

**Paula Raposo** – *C<sup>2</sup>TN – Centro de Ciências e Tecnologias Nucleares Instituto Superior Técnico, Universidade de Lisboa, 2695-066 Bobadela LRS, Portugal; DECN – Departamento de Engenharia e Ciências Nucleares, Instituto Superior Técnico, Universidade de Lisboa, 2695-066 Bobadela LRS, Portugal*

**Frederik Cleeren** – *Laboratory for Radiopharmaceutical Research, Department of Pharmacy and Pharmacology, University of Leuven, B-3000 Leuven, Belgium; [orcid.org/0000-0002-3692-1608](https://orcid.org/0000-0002-3692-1608)*

**Irwin Cassells** – *Laboratory for Radiopharmaceutical Research, Department of Pharmacy and Pharmacology, University of Leuven, B-3000 Leuven, Belgium; Nuclear Medical Applications, Belgian Nuclear Research Centre (SCK CEN), 2400 Mol, Belgium*

**Simon Leekens** – *Laboratory for Radiopharmaceutical Research, Department of Pharmacy and Pharmacology, University of Leuven, B-3000 Leuven, Belgium*

**Christopher Cawthorne** – *Nuclear Medicine and Molecular Imaging, Department of Imaging and Pathology, University of Leuven, 3000 Leuven, Belgium; [orcid.org/0000-0002-5975-0354](https://orcid.org/0000-0002-5975-0354)*

**Filipa Mendes** – *C<sup>2</sup>TN – Centro de Ciências e Tecnologias Nucleares Instituto Superior Técnico, Universidade de Lisboa, 2695-066 Bobadela LRS, Portugal; DECN – Departamento de Engenharia e Ciências Nucleares, Instituto Superior Técnico, Universidade de Lisboa, 2695-066 Bobadela LRS, Portugal; [orcid.org/0000-0003-0646-1687](https://orcid.org/0000-0003-0646-1687)*

**Célia Fernandes** – *C<sup>2</sup>TN – Centro de Ciências e Tecnologias Nucleares Instituto Superior Técnico, Universidade de Lisboa, 2695-066 Bobadela LRS, Portugal; DECN – Departamento de Engenharia e Ciências Nucleares, Instituto Superior Técnico, Universidade de Lisboa, 2695-066 Bobadela LRS, Portugal*

Complete contact information is available at:

<https://pubs.acs.org/10.1021/acs.molpharmaceut.3c00787>

## Notes

The authors declare no competing financial interest.

## ■ ACKNOWLEDGMENTS

This work was supported by Fundação para a Ciência e Tecnologia, Portugal (projects UID/Multi/04349/2019 and PTDC/MED-QUI/1554/2020), and received funding from the European Union's Horizon 2020 research and innovation programme under grant agreement no. 101008571 (PRISMAP – The European medical radionuclides programme).

## ■ REFERENCES

- (1) Sgouros, G.; Bodei, L.; McDevitt, M. R.; Nedrow, J. R. Radiopharmaceutical Therapy in Cancer: Clinical Advances and Challenges. *Nat. Rev. Drug Discov* **2020**, *19* (9), 589–608.
- (2) Bodei, L.; Herrmann, K.; Schöder, H.; Scott, A. M.; Lewis, J. S. Radiotheranostics in Oncology: Current Challenges and Emerging Opportunities. *Nat. Rev. Clin Oncol* **2022**, *19* (8), 534–550.
- (3) Ruigrok, E. A. M.; Van Weerden, W. M.; Nonnekens, J.; De Jong, M. The Future of PSMA-Targeted Radionuclide Therapy: An Overview of Recent Preclinical Research. *Pharmaceutics* **2019**, *11* (11), 560.
- (4) Rasul, S.; Hacker, M.; Kretschmer-Chott, E.; Leisser, A.; Grubmüller, B.; Kramer, G.; Shariat, S.; Wadsak, W.; Mitterhauser, M.; Hartenbach, M.; Haug, A. R. Clinical Outcome of Standardized <sup>177</sup>Lu-PSMA-617 Therapy in Metastatic Prostate Cancer Patients Receiving 7400 MBq Every 4 Weeks. *Eur. J. Nucl. Med. Mol. Imaging* **2020**, *47* (3), 713–720.
- (5) Kratochwil, C.; Bruchertseifer, F.; Giesel, F. L.; Weis, M.; Verburg, F. A.; Mottaghy, F.; Kopka, K.; Apostolidis, C.; Haberkorn, U.; Morgenstern, A. <sup>225</sup>Ac-PSMA-617 for PSMA-Targeted  $\alpha$ -Radiation Therapy of Metastatic Castration-Resistant Prostate Cancer. *J. Nucl. Med.* **2016**, *57* (12), 1941–1944.
- (6) Ku, A.; Facca, V. J.; Cai, Z.; Reilly, R. M. Auger Electrons for Cancer Therapy – a Review. *EJNMMI Radiopharm Chem.* **2019**, *4* (1), 27.
- (7) Bolcaen, J.; Gizawy, M. A.; Terry, S. Y. A.; Paulo, A.; Cornelissen, B.; Korde, A.; Engle, J.; Radchenko, V.; Howell, R. W. Marshalling the Potential of Auger Electron Radiopharmaceutical Therapy. *J. Nucl. Med.* **2023**, *64* (9), 1344–1351.
- (8) Valkema, R.; De Jong, M.; Bakker, W. H.; Breeman, W. A. P.; Kooij, P. P. M.; Lugtenburg, P. J.; De Jong, F. H.; Christiansen, A.; Kam, B. L. R.; De Herder, W. W.; Stridsberg, M.; Lindemans, J.; Ensing, G.; Krenning, E. P. Phase I Study of Peptide Receptor Radionuclide

- Therapy With [ $^{111}\text{In}$ -DTPA0]Octreotide: The Rotterdam Experience. *Semin. Nucl. Med.* **2002**, *32* (2), 110–122.
- (9) Anthony, L. B.; Woltering, E. A.; Espenan, G. D.; Cronin, M. D.; Maloney, T. J.; Mccarthy, K. E. Indium-111-Pentetreotide Prolongs Survival in Gastroenteropancreatic Malignancies. *Semin. Nucl. Med.* **2002**, *32* (2), 123–132.
- (10) Buscombe, J. R.; Caplin, M. E.; Hilson, A. J. W. Long-Term Efficacy of High-Activity  $^{111}\text{In}$ -Pentetreotide Therapy in Patients with Disseminated Neuroendocrine Tumors. *J. Nucl. Med.* **2003**, *44* (1), 1–6.
- (11) Limouris, G. S.; Chatziioannou, A.; Kontogeorgakos, D.; Mourikis, D.; Lyra, M.; Dimitriou, P.; Stavrika, A.; Gouliamos, A.; Vlahos, L. Selective Hepatic Arterial Infusion of In-111-DTPA-Phe1-Octreotide in Neuroendocrine Liver Metastases. *Eur. J. Nucl. Med. Mol. Imaging* **2008**, *35* (10), 1827–1837.
- (12) Vallis, K. A.; Reilly, R. M.; Scollard, D.; Merante, P.; Brade, A.; Velauthapillai, S.; Caldwell, C.; Chan, I.; Freeman, M.; Lockwood, G.; Miller, N. A.; Cornelissen, B.; Petronis, J.; Sabate, K. Phase I Trial to Evaluate the Tumor and Normal Tissue Uptake, Radiation Dosimetry and Safety of  $^{111}\text{In}$ -DTPA-Human Epidermal Growth Factor in Patients with Metastatic EGFR-Positive Breast Cancer. *Am. J. Nucl. Med. Mol. Imaging* **2014**, *4* (2), 181–192.
- (13) Borgna, F.; Haller, S.; Rodriguez, J. M. M.; Ginj, M.; Grundler, P. V.; Zeevaart, J. R.; Köster, U.; Schibli, R.; van der Meulen, N. P.; Müller, C. Combination of Terbium-161 with Somatostatin Receptor Antagonists—a Potential Paradigm Shift for the Treatment of Neuroendocrine Neoplasms. *Eur. J. Nucl. Med. Mol. Imaging* **2022**, *49* (4), 1113–1126.
- (14) Combined Beta- Plus Auger Electron Therapy Using a Novel Somatostatin Receptor Subtype 2 Antagonist Labeled With Terbium-161 ( $^{161}\text{Tb}$ -DOTA-LM3) (Beta plus). <https://clinicaltrials.gov/ct2/show/NCT05359146> (accessed 2023/10/27).
- (15) Hindie, E.; Zanotti-Fregonara, P.; Quinto, M. A.; Morgat, C.; Champion, C. Dose Deposits from  $^{90}\text{Y}$ ,  $^{177}\text{Lu}$ ,  $^{111}\text{In}$ , and  $^{161}\text{Tb}$  in Micrometastases of Various Sizes: Implications for Radiopharmaceutical Therapy. *J. Nucl. Med.* **2016**, *57* (5), 759–764.
- (16) Alcocer-Ávila, M. E.; Ferreira, A.; Quinto, M. A.; Morgat, C.; Hindie, E.; Champion, C. Radiation Doses from  $^{161}\text{Tb}$  and  $^{177}\text{Lu}$  in Single Tumour Cells and Micrometastases. *EJNMMI Phys.* **2020**, *7* (1), 33.
- (17) Bavelaar, B. M.; Lee, B. Q.; Gill, M. R.; Falzone, N.; Vallis, K. A. Subcellular Targeting of Theranostic Radionuclides. *Front. Pharmacol.* **2018**, *9*, 996.
- (18) Rosenkranz, A. A.; Slastnikova, T. A.; Georgiev, G. P.; Zalutsky, M. R.; Sobolev, A. S. Delivery Systems Exploiting Natural Cell Transport Processes of Macromolecules for Intracellular Targeting of Auger Electron Emitters. *Nucl. Med. Biol.* **2020**, *80–81*, 45–56.
- (19) Paillas, S.; Ladjohououl, R.; Lozza, C.; Pichard, A.; Boudousq, V.; Jarlier, M.; Sevestre, S.; Le Blay, M.; Deshayes, E.; Sosabowski, J.; Chardès, T.; Navarro-Teulon, I.; Mairs, R. J.; Pouget, J. P. Localized Irradiation of Cell Membrane by Auger Electrons Is Cytotoxic Through Oxidative Stress-Mediated Nontargeted Effects. *Antioxid Redox Signal* **2016**, *25* (8), 467–484.
- (20) Pouget, J. P.; Lozza, C.; Deshayes, E.; Boudousq, V.; Navarro-Teulon, I. Introduction to Radiobiology of Targeted Radionuclide Therapy. *Front Med. (Lausanne)* **2015**, *2* (MAR), 12.
- (21) Averbeck, D.; Rodriguez-Lafresse, C. Role of Mitochondria in IR Responses: Epigenetic, Metabolic, and Signaling Impacts. *Int. J. Mol. Sci.* **2021**, *22* (20), 11047.
- (22) Richardson, R. B.; Harper, M.-E. Mitochondrial Stress Controls the Radiosensitivity of the Oxygen Effect: Implications for Radiotherapy. *Oncotarget* **2016**, *7* (16), 21469–21483.
- (23) Kobashigawa, S.; Kashino, G.; Suzuki, K.; Yamashita, S.; Mori, H. Ionizing Radiation-Induced Cell Death Is Partly Caused by Increase of Mitochondrial Reactive Oxygen Species in Normal Human Fibroblast Cells. *Radiat. Res.* **2015**, *183* (4), 455–464.
- (24) Figueiredo, D.; Fernandes, C.; Silva, F.; Palma, E.; Rapisinho, P.; Belchior, A.; Vaz, P.; Paulo, A. Synthesis and Biological Evaluation of  $^{99\text{mTc}}$ (I) Tricarbonyl Complexes Dual-Targeted at Tumoral Mitochondria. *Molecules* **2021**, *26* (2), 441.
- (25) Fernandes, C.; Palma, E.; Silva, F.; Belchior, A.; Pinto, C. I. G.; Guerreiro, J. F.; Botelho, H. M.; Mendes, F.; Rapisinho, P.; Paulo, A. Searching for a Paradigm Shift in Auger-Electron Cancer Therapy with Tumor-Specific Radiopeptides Targeting the Mitochondria and/or the Cell Nucleus. *Int. J. Mol. Sci.* **2022**, *23* (13), 7238.
- (26) Kostelnik, T. I.; Orvig, C. Radioactive Main Group and Rare Earth Metals for Imaging and Therapy. *Chem. Rev.* **2019**, *119* (2), 902–956.
- (27) Kuo, H. T.; Merckens, H.; Zhang, Z.; Uribe, C. F.; Lau, J.; Zhang, C.; Colpo, N.; Lin, K. S.; Bénard, F. Enhancing Treatment Efficacy of  $^{177}\text{Lu}$ -PSMA-617 with the Conjugation of an Albumin-Binding Motif: Preclinical Dosimetry and Endoradiotherapy Studies. *Mol. Pharmaceutics* **2018**, *15* (11), S183–S191.
- (28) Deberle, L. M.; Benešová, M.; Umbricht, C. A.; Borgna, F.; Büchler, M.; Zhernosekov, K.; Schibli, R.; Müller, C. Development of a New Class of PSMA Radioligands Comprising Ibuprofen as an Albumin-Binding Entity. *Theranostics* **2020**, *10* (4), 1678–1693.
- (29) Scheiner, M.; Hoffmann, M.; He, F.; Poeta, E.; Chatonnet, A.; Monti, B.; Maurice, T.; Decker, M. Selective Pseudo-Irreversible Butyrylcholinesterase Inhibitors Transferring Antioxidant Moieties to the Enzyme Show Pronounced Neuroprotective Efficacy In Vitro and In Vivo in an Alzheimer's Disease Mouse Model. *J. Med. Chem.* **2021**, *64* (13), 9302–9320.
- (30) dos Santos, J. C.; Schäfer, M.; Bauder-Wüst, U.; Beijer, B.; Eder, M.; Leotta, K.; Kleist, C.; Meyer, J. P.; Dilling, T. R.; Lewis, J. S. Refined Chelator Spacer Moieties Ameliorate the Pharmacokinetics of PSMA-617. *Front. Chem.* **2022**, *10*, 898692.
- (31) Zielonka, J.; Joseph, J.; Sikora, A.; Hardy, M.; Ouari, O.; Vasquez-Vivar, J.; Cheng, G.; Lopez, M.; Kalyanaraman, B. Mitochondria-Targeted Triphenylphosphonium-Based Compounds: Syntheses, Mechanisms of Action, and Therapeutic and Diagnostic Applications. *Chem. Rev.* **2017**, *117* (15), 10043–10120.
- (32) Sulaimon, L. A.; Afolabi, L. O.; Adisa, R. A.; Ayankojo, A. G.; Afolabi, M. O.; Adewolu, A. M.; Wan, X. Pharmacological Significance of MitoQ in Ameliorating Mitochondria-Related Diseases. *Advances in Redox Research* **2022**, *5*, No. 100037.
- (33) Singh, R.; Setiady, Y. Y.; Ponte, J.; Kovtun, Y. V.; Lai, K. C.; Hong, E. E.; Fishkin, N.; Dong, L.; Jones, G. E.; Coccia, J. A.; Lanieri, L.; Veale, K.; Costoplus, J. A.; Skaletskaya, A.; Gabriel, R.; Salomon, P.; Wu, R.; Qiu, Q.; Erickson, H. K.; Lambert, J. M.; Chari, R. V. J.; Widdison, W. C. A New Triglycyl Peptide Linker for Antibody-Drug Conjugates (ADCs) with Improved Targeted Killing of Cancer Cells. *Mol. Cancer Ther.* **2016**, *15* (6), 1311–1320.
- (34) Bargh, J. D.; Isidro-Llobet, A.; Parker, J. S.; Spring, D. R. Cleavable Linkers in Antibody-Drug Conjugates. *Chem. Soc. Rev.* **2019**, *48* (16), 4361–4374.
- (35) Vultros, F.; Fernandes, C.; Mendes, F.; Marques, F.; Correia, J. D. G.; Santos, I.; Gano, L. A Multifunctional Radiotheranostic Agent for Dual Targeting of Breast Cancer Cells. *ChemMedChem.* **2017**, *12* (14), 1103–1107.
- (36) Hoffman, T. J.; Volkert, W. A.; Troutner, D. E.; Holmes, R. A. Reversed-Phase HPLC of [ $^{99\text{mTc}}$ ] Tetraamine Complexes. *Inn. J. Appl. Radiat. Isot.* **1984**, *35* (3), 223–225.
- (37) Banerjee, S. R.; Foss, C. A.; Castanares, M.; Mease, R. C.; Byun, Y.; Fox, J. J.; Hilton, J.; Lupold, S. E.; Kozikowski, A. P.; Pomper, M. G. Synthesis and Evaluation of Technetium-99m and Rhenium-Labeled Inhibitors of the Prostate-Specific Membrane Antigen (PSMA). *J. Med. Chem.* **2008**, *51* (15), 4504–4517.
- (38) Franken, N. A. P.; Rodermond, H. M.; Stap, J.; Haveman, J.; van Bree, C. Clonogenic Assay of Cells In Vitro. *Nat. Protoc.* **2006**, *1* (5), 2315–2319.
- (39) Garnuszek, P.; Karczmarczyk, U.; Maurin, M.; Sikora, A.; Zaborniak, J.; Pijarowska-Kruszyna, J.; Jaroń, A.; Wyczółkowska, M.; Wojdowska, W.; Pawlak, D.; et al. PSMA-D4 Radioligand for Targeted Therapy of Prostate Cancer: Synthesis, Characteristics and Preliminary Assessment of Biological Properties. *Int. J. Mol. Sci.* **2021**, *22* (5), 2731.

(40) Benešová, M.; Bauder-Wüst, U.; Schäfer, M.; Klika, K. D.; Mier, W.; Haberkorn, U.; Kopka, K.; Eder, M. Linker Modification Strategies to Control the Prostate-Specific Membrane Antigen (PSMA)-Targeting and Pharmacokinetic Properties of DOTA-Conjugated PSMA Inhibitors. *J. Med. Chem.* **2016**, *59* (5), 1761–1775.

(41) Derks, Y. H. W.; Rijpkema, M.; Amadajais-Groenen, H. I. V.; Loeff, C. C.; de Rooode, K. E.; Kip, A.; Laverman, P.; Lütje, S.; Heskamp, S.; Löwik, D. W. P. M. Strain-Promoted Azide–Alkyne Cycloaddition-Based PSMA-Targeting Ligands for Multimodal Intraoperative Tumor Detection of Prostate Cancer. *Bioconjug Chem.* **2022**, *33* (1), 194–205.

(42) Weineisen, M.; Simecek, J.; Schottelius, M.; Schwaiger, M.; Wester, H. J. Synthesis and Preclinical Evaluation of DOTAGA-Conjugated PSMA Ligands for Functional Imaging and Endoradiotherapy of Prostate Cancer. *EJNMMI Res.* **2014**, *4* (1), 63.

(43) Tschan, V. J.; Borgna, F.; Schibli, R.; Müller, C. Impact of the Mouse Model and Molar Amount of Injected Ligand on the Tissue Distribution Profile of PSMA Radioligands. *Eur. J. Nucl. Med. Mol. Imaging* **2022**, *49* (2), 470–480.

(44) Kalidindi, T. M.; Lee, S.-G.; Jou, K.; Chakraborty, G.; Skafida, M.; Tagawa, S. T.; Bander, N. H.; Schoder, H.; Bodei, L.; Pandit-Taskar, N.; et al. A Simple Strategy to Reduce the Salivary Gland and Kidney Uptake of PSMA-Targeting Small Molecule Radiopharmaceuticals. *Eur. J. Nucl. Med. Mol. Imaging* **2021**, *48* (8), 2642–2651.

(45) Matsui, T.; Nuryadi, E.; Komatsu, S.; Hirota, Y.; Shibata, A.; Oike, T.; Nakano, T. Robustness of Clonogenic Assays as a Biomarker for Cancer Cell Radiosensitivity. *Int. J. Mol. Sci.* **2019**, *20* (17), 4148.

(46) Matthias, J.; Engelhardt, J.; Schäfer, M.; Bauder-Wüst, U.; Meyer, P. T.; Haberkorn, U.; Eder, M.; Kopka, K.; Hell, S. W.; Eder, A.-C. Cytoplasmic Localization of Prostate-Specific Membrane Antigen Inhibitors May Confer Advantages for Targeted Cancer Therapies. *Cancer Res.* **2021**, *81* (8), 2234–2245.

(47) Shen, C. J.; Minn, I.; Hobbs, R. F.; Chen, Y.; Josefsson, A.; Brummet, M.; Banerjee, S. R.; Brayton, C. F.; Mease, R. C.; Pomper, M. G.; Kiess, A. P. Auger Radiopharmaceutical Therapy Targeting Prostate-Specific Membrane Antigen in a Micrometastatic Model of Prostate Cancer. *Theranostics* **2020**, *10* (7), 2888–2896.

(48) Kiess, A. P.; Minn, I.; Chen, Y.; Hobbs, R.; Sgouros, G.; Mease, R. C.; Pullambhatla, M.; Shen, C. J.; Foss, C. A.; Pomper, M. G. Auger Radiopharmaceutical Therapy Targeting Prostate-Specific Membrane Antigen. *J. Nucl. Med.* **2015**, *56* (9), 1401–1407.

(49) Haller, S.; Pellegrini, G.; Vermeulen, C.; van der Meulen, N. P.; Köster, U.; Bernhardt, P.; Schibli, R.; Müller, C. Contribution of Auger/Conversion Electrons to Renal Side Effects after Radionuclide Therapy: Preclinical Comparison of <sup>161</sup>Tb-Folate and <sup>177</sup>Lu-Folate. *EJNMMI Res.* **2016**, *6* (1), 13.

(50) Hu, Q.; Padron, K.; Hara, D.; Shi, J.; Pollack, A.; Prabhakar, R.; Tao, W. Interactions of Urea-Based Inhibitors with Prostate-Specific Membrane Antigen for Boron Neutron Capture Therapy. *ACS Omega* **2021**, *6* (49), 33354–33369.

(51) Lundmark, F.; Olanders, G.; Rinne, S. S.; Abouzayed, A.; Orlova, A.; Rosenström, U. Design, Synthesis, and Evaluation of Linker-Optimised PSMA-Targeting Radioligands. *Pharmaceutics* **2022**, *14* (5), 1098.

(52) Davis, M. I.; Bennett, M. J.; Thomas, L. M.; Bjorkman, P. J. Crystal Structure of Prostate-Specific Membrane Antigen, a Tumor Marker and Peptidase. *Proc. Natl. Acad. Sci. U S A* **2005**, *102* (17), 5981–5986.

(53) Kratochwil, C.; Giesel, F. L.; Leotta, K.; Eder, M.; Hoppe-Tich, T.; Youssoufian, H.; Kopka, K.; Babich, J. W.; Haberkorn, U. PMPA for Nephroprotection in PSMA-Targeted Radionuclide Therapy of Prostate Cancer. *J. Nucl. Med.* **2015**, *56* (2), 293–298.

(54) Rousseau, E.; Lau, J.; Kuo, H. T.; Zhang, Z.; Merkens, H.; Hundal-Jabal, N.; Colpo, N.; Lin, K. S.; Bénard, F. Monosodium Glutamate Reduces <sup>68</sup>Ga-PSMA-11 Uptake in Salivary Glands and Kidneys in a Preclinical Prostate Cancer Model. *J. Nucl. Med.* **2018**, *59* (12), 1865–1868.